DTRA-TR-99-22

Technical Report

Development of Optical Stress Gauges for Use in Shock Wave Experiments

Approved for public release; distribution is unlimited.

September 2000

Prepared for:
Defense Threat Reduction Agency
45045 Aviation Drive
Dulles, VA 20166-7517

DNA 001-92-C-0063

Yogendra M. Gupta

Prepared by: Washington State University
Department of Physics
Pullman, WA 99164-2814

DESTRUCTION NOTICE:

Destroy this report when it is no longer needed. Do not return to sender.

PLEASE NOTIFY THE DEFENSE THREAT REDUCTION AGENCY, ATTN: ADM, 45045 AVIATION DRIVE, DULLES, VA 20166-7517, IF YOUR ADDRESS IS INCORRECT, IF YOU WISH IT DELETED FROM THE DISTRIBUTION LIST, OR IF THE ADDRESSEE IS NO LONGER EMPLOYED BY YOUR ORGANIZATION.

DISTRIBUTION LIST UPDATE

This mailer is provided to enable DTRA to maintain current distribution lists for reports. (We would appreciate you providing the requested information.)

- ❑ Add the individual listed to your distribution list.
- ❑ Delete the cited organization/individual.
- ❑ Change of address.

Note:
Please return the mailing label from the document so that any additions, changes, corrections or deletions can be made easily. For distribution cancellation or more information call DTRA/ADM (703) 325-1036.

NAME: _____

ORGANIZATION: _____

OLD ADDRESS	NEW ADDRESS
_____	_____
_____	_____
_____	_____

TELEPHONE NUMBER: ( ) _____

DTRA PUBLICATION NUMBER/TITLE	CHANGES/DELETIONS/ADDITIONS, etc.) *(Attach Sheet if more Space is Required)*
_____	_____
_____	_____
_____	_____

DTRA or other GOVERNMENT CONTRACT NUMBER: _____

CERTIFICATION of NEED-TO-KNOW BY GOVERNMENT SPONSOR (if other than DTRA):

SPONSORING ORGANIZATION: _____

CONTRACTING OFFICER or REPRESENTATIVE: _____

SIGNATURE: _____

CUT HERE AND RETURN

REPORT DOCUMENTATION PAGE

FORM APPROVED
OMB No. 0704-0188

1. AGENCY USE ONLY	2. REPORT DATE	3. REPORT TYPE AND DATES COVERED
		Technical 920816-970630

4. TITLE AND SUBTITLE
Development of Optical Stress Gauges for Use in Shock Wave Experiments

5. Funding Numbers
C - DNA 001-92-C-0063
PE - 62715H
PR - AA
TA - EA
WU - DH00006

6. AUTHOR(S)
Yogendra M. Gupta

7. PERFORMING ORGANIZATION NAMES(S) AND ADDRESS(ES)
Washington State University
Department of Physics
Pullman, WA 99164-2814

8. PERFORMING ORGANIZATION REPORT NUMBER
990188-51201-FTR

9. SPONSORING / MONITORING GENCY NAMES(S) AND ADDRESS(ES)
Defense Threat Reduction Agency
45045 Aviation Drive
Dulles, VA 20166-7517
CPTIE / Kreutzian

10. SPONSORING / MONITORING AGENCY REPORT NUMBER
DTRA-TR-99-22

11. SUPPLEMENTARY NOTES
This work was sponsored by the Defense Threat Reduction Agency under RDT&E RMC code B4662 D AA EA 00006 5200 A AA 25904D.

a. DISTRIBUTION / AVAILABILITY STATEMENT
Approved for public release; distribution is unlimited.

12. DISTRIBUTION CODE

13. ABSTRACT (Maximum 200 words)

Experiments and analyses were carried out to demonstrate the successful development and use of the ruby stress gauges under shock wave loading. The predictive capability of our theoretical model, developed earlier, was established by the good agreement obtained between the calculated and measured R-line shifts for shock wave compression of r-cut samples. The feasibility of using stimulated emission to enhance the signal intensity from shocked ruby crystals was demonstrated.

The major element of the present work involved the successful development and use of in-situ, miniature ruby sensors in high stress and high strain rate environments. The miniature ruby sensors developed have provided good quality signals in a wide variety of materials (metals, polymers, eramics and geologic solids) shocked to stresses ranging from 0.3 to 8.0 GPa. Additionally, the ability of the miniature ruby sensors to provide quantitative, time-resolved data under 2-D, dynamic loading is expected to be valuable in obtaining stress measurements in a wide variety of applications involving rapid impulsive loading. The use of R2-line shifts to obtain the mean stress will be useful for material property studies under dynamic loading .

14. SUBJECT TERMS
Stress Gauge, R-Lines, Shock Waves, Optical Sensor
Fiber Optics, High Stress, Dynamic Loading, Ruby Luminescence

15. NUMBER OF PAGES
52

16. PRICE CODE

17. SECURITY CLASSIFICATION OF REPORT	18. SECURITY CLASSIFICATION OF THIS PAGE	19. SECURITY CLASSIFICATION OF ABSTRACT	20. LIMITATION OF ABSTRACT
UNCLASSIFIED	UNCLASSIFIED	UNCLASSIFIED	SAR

SUMMARY

The overall goal of the present work was to demonstrate the successful development and use of an optical stress gauge for time-resolved stress measurements in shock wave experiments. The work described in this report represents the culmination of a comprehensive research effort that demonstrated the transition of a novel scientific concept to a usable stress gauge.

In the first part of our work, we demonstrated the predictive capability of our piezoluminescence model developed in our earlier work. We conducted plate impact experiments to determine the shift of ruby R-lines in r-cut samples subjected to uniaxial strain. Since our theoretical model had been developed entirely from experiments on c-cut and a-cut samples, the experimental results from r-cut samples provided a valuable check on the model predictions. The good agreement between the theory and experiments was gratifying and demonstrates that our theoretical model can be used with good confidence.

In another part of our work, we examined the feasibility of increasing the signal intensity from ruby gauges using stimulated emission. In single event, time-resolved measurements, increasing the signal-to-noise ratio is an ongoing, important need. We carried out theoretical analyses to determine the signal gain for the particular experimental configurations of interest. Subsequently, experimental measurements of the signal gain were obtained at ambient conditions and under shock loading. Good agreement was obtained between the calculated and the measured signal gain. Hence, the use of stimulated emission needs to be explored in future experiments.

The major part of the present work involved an experimental effort to develop and use miniature ruby sensors (400 μm to 1000 μm in diameter and 250 μm thick) in a wide variety of materials (metals, polymers, ceramics, and geologic solids) subjected to high stress and high strain loading using plate impact experiments. A considerable effort was spent in developing the experimental methods that would permit the fabrication and use of ruby sensors for in-situ, stress gauges in shocked materials. Good quality

signals were obtained at stresses ranging from 0.3 GPa to 8 GPa in shocked materials. Ruby gauges provided quantitative data during loading and unloading, and for time durations in excess of 5 μs. The ability to get good data under 2-D loading was also demonstrated. This development is expected to be valuable for many applications involving rapid impulsive loading.

The long term objective of having a reliable, purely optical stress transducer for time-resolved measurements under dynamic loading was completed successfully. Starting with a novel scientific concept and through sustained experimental and theoretical efforts, a practical and useful optical stress gauge has been developed.

The next step would be to use these gauges in various applications to establish the experimental limits of their usage. Most importantly, a careful analytic/numerical effort needs to be undertaken to develop accurate procedures to invert the gauge output in a meaningful manner.

PREFACE

This report describes a research effort sponsored by the Defense Threat Reduction Agency (DTRA) (the Defense Nuclear Agency, later renamed the Defense Special Weapons Agency, consolidated into DTRA) under contract DNA 011-92-C-0063. The project monitor, Mr. M. Flohr, is sincerely thanked for his support and interest in this effort. Mr. T. Kennedy is also thanked for his support and encouragement of the optical stress sensor development.

The author gratefully acknowledges the efforts of many dedicated coworkers (K. A. Zimmerman, S. M. Sharma, J. K. Hyun, M. D. Knudson, A. Brown, C. P. Constantinou, and R. Feng), who contributed to the success of this work. In particular, K. A. Zimmerman is commended for his outstanding experimental contributions to the miniature ruby gauge development. D. Savage assisted with the impact experiments and D. Krakowski assisted with the report preparation; they are thanked for the same.

CONVERSION TABLE

Conversion factors for U.S. Customary to metric (SI) units of measurement.

MULTIPLY →	BY →	TO GET
TO GET ←	BY ←	DIVIDE

angstrom	1.000 000 X E -10	meters (m)
atmosphere (normal)	1.013 25 X E +2	kilo pascal (kPa)
bar	1.000 000 X E +2	kilo pascal (kPa)
barn	1.000 000 E -28	meter^2 (m^2)
British thermal unit (thermochemical)	1.054 350 X E +3	joule (J)
calorie (thermochemical)	4.184 000	joule (J)
cal (thermochemical/cm^2)	4.184 000 X E -2	mega joule/m2 (MJ/m^2)
curie	3.700 000 X E +1	*giga becquerel (BGq)
degree (angle	1.745 329 X E -2	radian (rad)
degree Fahrenheit	$t_k = (t^0f + 459.67)/1.8$	degree kelvin (K)
electron volt	1.602 19 X E -19	joule (J)
erg	1.000 000 X E -7	joule (J)
erg/second	1.000 000 X E -7	watt (W)
foot	3.048 000 X E -1	meter (m)
foot-pound-force	1.355 818	joule (J)
gallon (U.S. liquid)	3.785 412 X E -3	meter^3 (m^3)
inch	2.540 000 X E -2	meter (m)
jerk	1.000 000 X E +9	joule (J)
joule/kilogram (J/kg) radiation dose absorbed	1.000 000	Gray (Gy)
kilotons	4.183	terajoules
kip (1000 lbf)	4.448 222 X E +3	newton (N)
kig/inch^2 (ksi)	6.894 757 X E +3	kilo pascal (kPa)
ktap	1.000 000 X E +2	newton-seconds/m^2 ($N\text{-}s/m^2$)
micron	1.000 000 X E -6	meter (m)
mil	2.540 000 X E -5	meter (m)
mile (international)	1.609 344 X E +3	meter (m)
ounce	2.834 952 X E -2	kilogram (kg)
pound-force (lbs avoirdupois)	4,448 222	newton (N)
pound-force inch	1.129 848 X E -1	newton-meter ($N \cdot m$)
pound-force/inch	1.751 268 X E +2	newton/meter (N/m)
pound-force/foot^2	4.788 026 X E -2	kilo pascal (kPa)
pound-force/inch^2 (psi)	6.894 757	kilo pascal (kPa)
pound-mass (lbm avoirdupois)	4.535 924 X E -1	kilogram (kg)
pound-mass-foot^2 (moment of inertia)	4.214 011 X E -2	kilogram-meter^2 ($k \cdot gm^2$)
pound-mass/foot^3	1.601 846 X E +1	kilogram/meter^3 (kg/m^3)
rad (radiation dose absorbed)	1.000 000 X E -2	**Gray (Gy)
roentgen	2.579 760 X E -4	coulomb/kilogram (C/kg)
shake	1.000 000 X E -8	second (s)
slug	1.459 390 X E +1	kilogram (kg)
torr (mm Hg, 0^0 C)	1.333 22 X E -1	kilo pascal (kPa)

* The becquerel (Bq) is the SI unit of radioactivity: 1 Bq = 1 event/s.
** The Gray (Gy) is the SI unit of absorbed radiation.

TABLE OF CONTENTS

SECTION 1
INTRODUCTION

1.1 OBJECTIVES.

In our earlier work (carried out under DNA Contract 001-88-C-0070)*, we had carried out a comprehensive investigation to understand stress-induced changes in the ruby R-line spectrum under shock loading. The work described in this report builds on the earlier work to continue the development of an optical stress sensor for use under dynamic loading. The overall goal of the present work was to demonstrate the successful development and use of ruby gauges to obtain time-resolved stress measurements in shock wave experiments. The specific objectives of the present work were:

1. To examine the predictive capability of our piezoluminescence model by comparing theoretical predictions with experimental measurements of R-line shifts for shock loading along the low symmetry, r-direction.

2. To examine the feasibility of stimulated emission for measuring R-line shifts in shocked ruby; such a development would permit improved signal quality in applications.

3. To develop experimental methods that would permit the use of miniature ruby sensors for in-situ, stress measurements in shocked solids.

4. To demonstrate the use of miniature ruby gauges for measuring stresses during loading and unloading in a variety of materials.

5. To examine the issues associated with inverting the ruby data to determine sample stresses.

The above list of objectives was designed to develop a practical, in-situ optical stress gauge that could be used in a wide variety of materials subjected to dynamic loading. A

* To facilitate the discussion in this report, the summary from our earlier report (DNA-TR-93-128) is presented as Section 1.2

significant fraction of the present work involved the development of successful experimental methods for using miniature ruby sensors.

1.2 SUMMARY OF PREVIOUS WORK (DNA-TR-93-128).

The overall goal of this work was to provide an in-depth understanding of stress-induced changes in the ruby R-line spectrum under shock loading. This goal completes the fundamental investigation, initiated at Washington State University, to develop an optical stress gauge that permits accurate, time-resolved stress measurements under dynamic loading conditions. The work described in this report represents an important step in making the transition from a scientific concept to a well characterized stress sensor.

In the first part of our work, we developed an experimental method to measure the wavelength shifts of the R-lines in ruby samples subjected to well defined, large tensile stresses. Plate impact experiments were used to produce uniaxial strain tension along the crystal c-axis. Peak longitudinal stresses up to 105 kbar were obtained in tension. Both R-lines remained sharp and showed a reversible, nonlinear blue shift in tension; for this orientation the $R_1 - R_2$ splitting increases with increasing tension. The ability to obtain quantitative data in tension is an important advantage for stress gauge applications.

In the second part of our work, we examined the effect of crystal orientation on ruby R-line shifts, under elastic compression and tension, by measuring shifts in crystals shocked along the a-axis and comparing these data with the shock data along the c-axis and hydrostatic measurements. The experimental results show strong anisotropy in R-line shifts for both compression and tension, and provide evidence for local symmetry changes under shock loading. The nonlinear increase in $R_1 - R_2$ splitting for both compression and tension is in marked contrast to the c-axis data. The strong anisotropy observed in the spectroscopy results is a novel finding because the continuum response of sapphire (or ruby) is isotropic. An interesting result from this work was the finding that the R_2-line shift depends on the density compression and is independent of nonhydrostatic stresses and crystal orientation.

In the next stage of our work, we extended the theoretical work of Sharma and Gupta [Phys. Rev. B **43**, 879 (1991)]. This earlier effort represented a conceptual breakthrough because it related the R-line shifts to different deformation conditions. The extension carried out in the current project permits an analysis of R-line shifts for any arbitrary deformation or crystal orientation as long as the crystal response is elastic. Thus, the theoretical developments permit a consistent analysis of all available shock, hydrostatic, and uniaxial – stress deformation data on R-line shifts.

In the next stage of our work, we undertook a comprehensive investigation of the R-line shifts at higher shock stresses. The specific objectives were to determine the upper stress limit for reversible (or elastic) response, and to determine the ability of the sensor to function beyond the elastic limit. Because spectral measurements during inelastic deformation require special considerations (large dynamic range for the detector, precise measurements of intensities, line broadening, and spectral structure), a significant effort was spent in modifying the recording system. These experimental developments turned out to be essential for the high stress work. The R-line data, in combination with some absorption data on sapphire (not reported here), suggest an elastic limit of 145-150 kbar for c-cut ruby and an elastic limit of approximately 170 kbar for a-cut ruby. Beyond the elastic limit (impact stress of 205 kbar assuming an elastic response), the changes in R-line spectra correspond to an elastic response (a discontinuous shift within experimental resolution) followed by stress relaxation and inelastic deformation. The a-cut crystals show rapid stress relaxation, considerable line broadening and structure, and strong hysteresis; essentially, the a-cut crystals are not usable beyond the elastic limit. In contrast, shock propagation along the c-axis results in slower stress relaxation, minimal line broadening, distinct R-lines and lower hysteresis. The optical quality of the data permits the use of the c-axis crystals beyond the elastic limit. Such usage will, however, need to incorporate hysteresis effects. The R-line spectra have provided information about the nature of inelastic deformation in shocked sapphire.

In the final stage of our work, we explored the use of developing sensors that may provide higher precision at low stresses (below 20 kbar). The preliminary experiments

described in our earlier report (DNA-TR-89-136) were modified to measure the time-resolved shift of the fluorescence spectrum of a dye (Rhodamine 6G) in ethanol subjected to shock wave, uniaxial strain loading. A nonlinear, red shift of the fluorescence band was observed between 2.6 and 19 kbar. These data show the potential of using this shift as an optical pressure sensor at low stresses (below 20 kbar) to complement the ruby sensor.

All of the objectives for the present work were successfully completed and the present results provide a good basis for shifting the focus of the work from characterizing and understanding the ruby response to using the ruby gauge for stress measurement applications.

SECTION 2
SYNOPSIS OF EXPERIMENTAL AND THEORETICAL DEVELOPMENTS

2.1 RUBY R-LINE SHIFTS FOR SHOCKED R-CUT CRYSTALS.

The successful development and use of an in-situ, ruby gauge requires that we have a rigorous understanding of the R-line shifts under arbitrary loading. Hence, we need to ascertain if our piezoluminescence model can be used to predict R-line shifts with good confidence.

The theoretical developments we had carried out were based on shock compression along the c and a axis. The developments were general enough to be applicable to any arbitrary strain state in the ruby. It was decided that shock compression along a low symmetry direction would provide a good test of the predictive capability of the model. Because they are readily available, we chose to examine r-cut crystals, that is, we undertook shock compression experiments along the $(1\bar{1}02)$ direction.

The theoretical formulation was used in conjunction with the nonlinear model parameters to predict ruby R-line shifts for shock compression along the r-direction. Predictions of R_1 shift, R_2 shift, and R_1-R_2splitting were compared with experimental measurements. Good agreement was observed between theory and experiments and a good case can be made for the predictive capability of our theoretical model.

During the present work, it was discovered that the elastic limit for shock propagation along the r axis was considerably smaller (~6.5 GPa) than that observed for c and a axis. This observation, initially surprising since no similar finding has been reported in the literature, was confirmed using quartz gauge measurements.

Details of this work may be seen in Appendix A.

2.2 FEASIBILITY OF STIMULATED EMISSION TO MEASURE R-LINE SHIFTS IN SHOCKED RUBY.

In all previous studies, ruby R-line shifts under shock compression and tension were measured using the spontaneous luminescence from optically pumped samples. The

signal intensities obtained through the use of this method are limited by the rather long lifetime of the ruby luminescence. The typical experimental duration ranges between 100 ns to several microseconds while the R-line luminescence lifetime is 3 ms. Hence, only a fraction of the energy stored is emitted in the experiment. Additionally, the emission fluoresces into all angles.

We investigated the use of stimulated emission to obtain higher intensities for measuring R-line shifts. Theoretical calculations were carried out to determine the magnitude of the signal gain for the particular experimental arrangements of interest in shock wave experiments. Experiments were then conducted at ambient conditions and under shock loading to measure the signal gain. Good agreement was obtained between the calculated signal gain and the experimentally measured signal gain. Hence, this work makes a good case for incorporating the stimulated emission technique for improved signal-to-noise ratio in measuring ruby R-line shifts in shock wave experiments.

Details of this work may be seen in Appendix B.

2.3 DEVELOPMENT AND USE OF MINIATURE RUBY SENSORS IN SHOCK WAVE EXPERIMENTS.

This effort comprised the major element of the present research project. *The successful development and use of ruby R-line shifts for in-situ, stress measurements in shocked materials has been the principal objective of our long term research effort supported by DNA.* This development marked the transition of a novel scientific concept to a practical, in-situ, optical stress sensor.

Throughout this work, the emphasis was on the development of a reliable ruby gauge which could be used in a wide variety of materials. A significant fraction of our effort was spent in developing experimental methods to prepare miniature ruby sensors, to mount them on optical fibers, to embed them in samples, and to obtain good quality data using these sensors in plate impact experiments.

We were successful in obtaining good quality data in a variety of representative materials: metal, polymer, ceramics, and a geologic solid. Good ruby data were obtained at stresses ranging from 0.3 GPa to 8 GPa and for time durations exceeding 5 μs. R-line shifts were obtained under both loading and unloading. An interesting and important observation was that the ruby gauges provide good data during 2-D loading conditions. This is an important finding since most applications involve non-planar loading. Because of the paucity of reliable stress sensors under non-planar loading, the ability to get good data under non-planar loading will be valuable for future work.

The size of the miniature ruby sensors and the fact that their mechanical response is elastic is beneficial for several reasons: sensor survival has a high probability; stress distributions at sub-mm length scales can be obtained; any hysteresis observed in the gauge data arises due to residual stresses in the sample. Of course, as always, the gauge-matrix interaction (or the inclusion problem) needs to be addressed to obtain sample stresses from the gauge output.

The principal perturbation to the sample stresses by the in-situ, gauge arises due to the presence of the optical fiber. The length scales over which these perturbations are significant can be reduced by using small fibers but the problem can not be eliminated. We emphasize that this problem is present in all in-material measurements, irrespective of the gauge type, to some degree.

Further details about this part of the work may be seen in Appendix C. An important result shown in the Appendix is the apparent finding of a single calibration curve for the R_2-line shift vs. sample mean stress in several different materials. While this result is very encouraging, further work is needed to establish the universality of this result.

To date, the miniature ruby gauges developed at Washington State University have produced good quality signals in a wide variety of materials shocked between 0.3 to 8 GPa. Hence, the development of the ruby gauge for dynamic loading has been completed successfully. This development is based on a strong experimental and

theoretical foundation, and the output from in-situ, ruby gauges can be used to check the material response of samples subjected to dynamic loading.

Future work needs to establish the experimental limits for stress bounds and to use them in various applications of interest.

2.4 ANALYSIS OF THE RUBY GAUGE DATA.

During the course of this work, we spent some effort to address the following problem: how to invert the ruby gauge data to obtain stresses in the samples? Essentially, this is the gauge-matrix interaction problem and a broad range of "forward solutions" need to be carried out to understand and address this problem. Toward this end, we have successfully worked out the analytic approaches to link our piezoluminescence model to a 2-D, finite difference code in which the ruby sensor and the optical fiber are modeled explicitly and with sufficient spatial resolution.

While the analytic/numerical approach to do the "forward solution" has been successfully developed, the resources in our research project did not permit us to complete the numerical analyses and to carry out the extensive calculations to fully address this need. The work to date should be considered as a good start but viewed as work in progress. *In our estimation, the most important future need is to carry out a wide range of numerical solutions in which the relevant parameters are varied systematically.* Such calculations, coupled with a small number of well designed experiments, will go a long way toward the reliable and routine use of the ruby sensor as an in-situ, stress gauge under dynamic loading. Given the considerable payoff in a wide variety of DOD applications, such an investment is well worth the effort.

SECTION 3
CONCLUSIONS

As stated in Section 1, the overall goal of the present work was to demonstrate the successful development and use of ruby gauges to obtain time-resolved stress measurements in shock wave or dynamic loading experiments. This goal has been met and good data from miniature ruby gauges have been obtained in the present work. The following specific objectives were completed:

1. The predictive capability of our piezoluminescence model was demonstrated by the calculations and measurements of R-line shifts for shock compression along the r-axis.

2. The feasibility of stimulated emission to enhance signal intensity associated with R-line shifts in shocked ruby was demonstrated.

3. An extensive effort was undertaken to work out and optimize experimental methods to develop miniature ruby sensors for use in shock wave experiments.

4. The use of miniature ruby sensors for in-situ, stress measurements was demonstrated for a wide variety of materials. Good data have been obtained in loading and unloading when samples were shocked to peak stresses ranging between 0.3 GPa and 8 GPa. Pulse durations in excess of 5 μs were recorded and we do not anticipate difficulties in recording data for 10 μs or longer.

5. The ability to get good data in 2-D loading was successfully demonstrated.

The present work represents the culmination of a sustained research effort which has resulted in the development of a purely optical stress gauge starting from a novel scientific concept. This development was based on fundamental research that combined careful experiments and rigorous analyses. All of this fundamental work has been published in peer reviewed journals. Future work should address how the ruby gauge data can be inverted routinely to obtain sample stresses.

APPENDIX A
RUBY R-LINE SHIFTS FOR SHOCK COMPRESSION ALONG (1102)

Jin-Kee Hyun,[a] Surinder M. Sharma,[b] and Y. M. Gupta[c]
Shock Dynamics Center and Department of Physics, Washington State University, Pullman, Washington 99164-2814

(Received 25 March 1998; accepted for publication 15 May 1998)

Experimental measurements of the shifts of ruby *R* lines, for shock loading along the low symmetry *r* direction, were obtained to evaluate our earlier theoretical formulation regarding the response of *R* lines in ruby crystals subjected to arbitrary deformations. The experimental results show good agreement with the calculated values based on symmetry adapted irreducible strains and, therefore, make a strong case for the predictive capability of the theoretical model. Additionally, the parameters in the theory were augmented to incorporate the previously observed nonlinear shifts of the *R* lines for shock compression along the *c* and *a* axis. With the general validation of our theoretical model, oriented ruby chips can now be utilized in diamond anvil cell experiments to obtain quantitative estimates of stress deviators at high pressures. These, in turn, can be used to evaluate material strength, and the role of nonhydrostatic stresses on sample response, at large compressions. © *1998 American Institute of Physics.* [S0021-8979(98)07716-0]

I. INTRODUCTION

The response of ruby *R* lines has been investigated carefully over the last several years in our laboratory by examining the shift of these lines when well-oriented crystals of ruby are shocked along the *c* and *a* axis.[1–5] Because the strain state is determined precisely in plane shock wave experiments, this approach provides an elegant way to correlate the macroscopic strain state of the crystal to the spectroscopic response of the *R* lines. The observed variations in the position of the *R* lines were analyzed quantitatively by Sharma and Gupta[3] in terms of a theoretical formulation, based on the symmetry changes around the Cr atom, that utilized symmetry adapted irreducible strains. This formulation is phenomenological since the parameters in the theoretical model were obtained partially from the experimental data. This theoretical formulation was further generalized by Shen and Gupta[4] to write the R_1-R_2 splitting matrix explicitly in terms of symmetry adapted strains.

In principle, the theoretical developments are general enough to be applicable to an arbitrary strain state in the ruby crystal, but so far they have been tested only for uniaxial strain loading along the *c* and *a* axis.[3–5] For a more general validation of the theory, it is necessary to examine the theoretical predictions against experimental observations for well-defined loading along orientations other than the *c* and *a* axis. Additionally, it would be more appropriate to test the theory when uniaxial strain is applied along a relatively low symmetry direction, because such a deformation will change the relative magnitude of the symmetry adapted strains significantly in contrast to uniaxial strain along the *c* and *a* axis. Therefore, we have carried out experiments where the ruby crystals were shocked along a (low symmetry) *r* direction, i.e., $(1\bar{1}02)$. In the present article, we compare the theoretical predictions and the experimental results for this orientation. In addition, the parameters in the theoretical model[3,4] have been modified to incorporate the observed nonlinear changes in the *R* line shifts,[1,4,5] as a function of strain, for shock compression along the *c* and *a* axis. This modification entailed the addition of a nonlinear term while retaining the earlier linear term. Addition of the nonlinear term has further improved the good agreement obtained previously between the theory and experiments along the *c* and *a* axis.[3–5] The comparison with the *r*-axis data presented here utilizes these parameters.

We emphasize that the present work, though utilizing shock wave experiments, is likely of most utility for static high pressure studies employing diamond anvil cells (DAC). Recently, there has been considerable interest in determining material strength under compression at high pressures (Refs. 6 and 7 and references therein). In these measurements, the stress deviators are evaluated using the equation of state of the material in quasihydrostatic compression.[8] This procedure is known to overestimate the stress deviators.[7] Thus, it will be useful to independently evaluate stress deviators at high pressures. If the theoretical model for determining the *R*-line response is shown to have predictive capability for uniaxial strain along an arbitrary orientation, then oriented ruby chips may be utilized for determining stress deviators at large compressions.

II. THEORETICAL FORMULATION

We briefly summarize the salient features of the theoretical model;[3,4] a detailed discussion may be seen in these references. The unperturbed Hamiltonian, for describing the electronic states representing the ruby *R* lines, assumes a hypothetical octahedral symmetry around the Cr atom. The perturbation Hamiltonian is taken as linearly proportional to the irreducible strains. It is further assumed that the strain

[a]Present address: Department of Chemistry and Biochemistry, University of Texas at Austin, Austin, TX 78712.
[b]Permanent address: High Pressure Physics Division, Bhabha Atomic Research Centre, Bombay 400 085, India.
[c]Electronic mail: shock@wsu.edu

induced changes in the Hamiltonian, for symmetry other than totally symmetric representation (A_1), are small enough to be treated by a second order perturbation theory. Symbolic representation of these statements is as follows (see Refs. 3 and 4 for more details):

$$H_{\text{strain}} = H_{A_1} + H_E + H_{T_2}, \tag{1}$$

$$H_{\text{pert}} = H_E + H_{T_2} + H_{\text{trig}}(\equiv V_{x0}^0) + H_{\text{so}}, \tag{2}$$

$$= V_{x0}^0 + (e_{x0} + e_{x+} + e_{x-}) V_{T_{2g}} + (e_{u+} + e_{u-}) V_E, \tag{3}$$

where A_1, E, and T_2 represent the three irreducible representations of the octahedral group; H_{trig} or V_{x0}^0 represents the ambient trigonal distortion of the octahedral arrangement at the Cr site; and H_{so} represents the spin-orbit coupling. $V_{T_{2g}}$ and V_E are parameters characteristic of rhombic and E distortions (one component of which is tetragonal[3]), respectively. Strains represented by e_{x+} and e_{x-} are rhombic, and those by e_{u+} and e_{u-} belong to E irreducible strain.[3] The strains of A_1 type, the uniform strains, are included in the unperturbed octahedral part of the Hamiltonian (H_0).

To write the symmetry adapted strains, we first transform the strains from the crystallographic frame to the local trigonal coordinate system.[3] The irreducible strains can then be written as follows

$$e(A_1) = e_{XX} + e_{YY} + e_{ZZ}, \tag{4}$$

$$e_{u+} = -e_{u-}^* = -\frac{1}{\sqrt{6}}[e_{XX} - e_{YY} - 2ie_{XY} + 2\sqrt{2}(e_{ZX} + ie_{ZY})], \tag{5}$$

$$e_{x+}(T_2) = -e_{x-}^*(T_2) = -\frac{1}{\sqrt{3}}\left[\frac{1}{2}(e_{XX} - e_{YY} - 2ie_{XY}) - \frac{1}{\sqrt{2}}(e_{ZX} + ie_{ZY})\right], \tag{6}$$

$$e_{x0}(T_2) = \frac{1}{2\sqrt{3}}(2e_{ZZ} - e_{XX} - e_{YY}), \tag{7}$$

where the strain terms on the right-hand side refer to the local trigonal coordinate system.[3]

The matrix describing the R_1, R_2 splitting, obtained using second order perturbation theory, has the following form:[4]

$$\begin{bmatrix} A & C & D & 0 \\ C^* & B & 0 & D \\ D^* & 0 & B & -C \\ 0 & D^* & -C^* & A \end{bmatrix}, \tag{8}$$

where

$$A = \frac{M + 2K\zeta}{A'},$$

$\zeta = 187\ \text{cm}^{-1}$ (spin-orbit coupling parameter),

$A' = \epsilon(^2E) - \epsilon(^2T_2) = -6734\ \text{cm}^{-1}$,

$M = 6K^2 + 12K_1^2|e_{x-}|^2$,

$K = K_0 + K_1 e_{x0}$,

$K_0 = -266.666\ \text{cm}^{-1}$ (ambient trigonal field parameter),

$$B = \frac{M - 2K}{A'},$$

$$C = \frac{2\sqrt{2}K_1 e_{x-}^*}{A'},$$

$$D = \frac{N}{A'} + qe_{u-},$$

$N = -12K_1 K e_{x-} - 6K_1^2(e_{x-}^*)^2$,

$q = Q/e_{u-}$ (the parameter related to E strains).

Parameters K_1 and q are derived from the response of R lines for shock compression along the c and a axis, respectively. K_0, ζ, and A' are derived from spectral data at ambient conditions. We also assume that ζ and A' do not change with compression. In principle these do vary but for the compression range of interest, the variations may be ignored.[3]

The eigenmatrix in Eq. (8) has two solutions, corresponding to the R_1 and R_2 lines,

$$\epsilon_{\pm} = \frac{(A+B) \pm [(A-B)^2 + 4(|C|^2 + |D|^2)]^{1/2}}{2} \tag{9}$$

The detailed form of $R_1 - R_2$ splitting can be written as[4]

$$\Delta(\epsilon_+ - \epsilon_-) = \left[\left(\frac{4K}{A'}\right)^2 + 2\left(\frac{4K_1}{A'}\right)^2 |e_{x-}^*|^2 + 4\left|qe_{u-} - \frac{12K_1 K e_{x-} + 6K_1^2(e_{x-}^*)^2}{A'}\right|^2\right]^{1/2}. \tag{10}$$

III. CHOICE OF PARAMETERS

Essentially, there are only three parameters which we need to know to calculate the shifts and splitting of R lines: $\Pi[e(A_1)]$ represents the shift due to uniform strain; K_1 gives the variation with respect to the T_2 rhombic strains; and the third one is the q parameter corresponding to the strains of E representation. Due to the strength of the ambient trigonal field in ruby, the trigonal field induced shift in the mean value of R_1 and R_2 may not agree with the predictions of perturbation theory. Hence, we introduced another parameter, $\Pi(e_{x0})$, for the shift caused by the variations in the trigonal field.[3] These parameters were evaluated in Refs. 3 and 4, and for completeness they are listed below:

Shift due to uniform strain, i.e., $\Pi[e(A_1)]$

$$= -1977.5\ \text{cm}^{-1}, \tag{11}$$

Change in the trigonal field/trigonal strain $= 3457\ \text{cm}^{-1}$, (12)

Shift due to trigonal strain $\Pi(e_{x0}) = 645.7e_{x0}\ \text{cm}^{-1}$, (13)

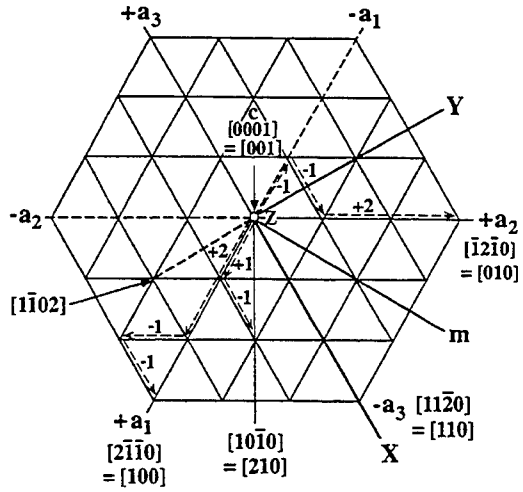

FIG. 1. Basal plane in ruby showing the relationship between the crystallographic (hexagonal) and local trigonal coordinate system (XYZ). The indices for the directions are with respect to crystallographic system. Also shown is a projection of the r-axis direction ($1\bar{1}02$) on the basal plane.

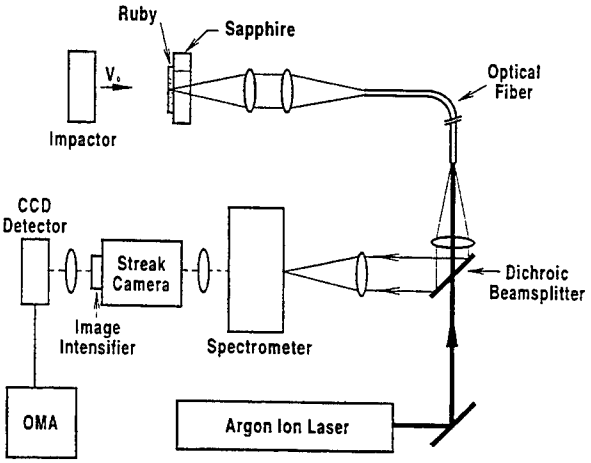

FIG. 2. Schematic view of the overall experimental arrangement.

value of q (two solutions)$=3183.8$ or -857 cm^{-1}. (14)

Nonlinear corrections: The above parameters were obtained from the data by assuming that for shock loading along the c axis the shifts and splittings are linear in strain while for shock loading along the a axis the mean of R_1 and R_2 shifts linearly with strain; note, for the evaluation of q this approximation was not made.[4] For small strains, this linear dependence is a good representation. At higher strains, the experimental data display a small curvature for shock loading along both the c and the a axis. From results along the c axis[1,2,5] and a axis,[4] the shift due to uniform strain can be written as

$$\Pi[e(A_1)] = -1977.5e(A_1) - 4360.6e^2(A_1). \quad (15)$$

Similarly, the shock response of R lines for shock loading along the c axis provides a nonlinear shift due to trigonal strain as

$$\Pi(e_{x0}) = 645.5e_{x0} - 35936.4e_{x0}^2. \quad (16)$$

Furthermore, the earlier estimate of K_1 was derived with the assumption that the variation in $R_2 - R_1$ splitting, due to the change in the trigonal field, was linear in strain for shock loading along the c axis. However, experimental results for tensile and compressive strain along the c axis indicate that there is a small nonlinear contribution. The experimental data along the c axis provide

$$K_1 = 3457 - 4776.16\mu, \quad (17)$$

where $\mu \equiv \rho/\rho_0 - 1$. With these nonlinear corrections, the q values were recalculated to match the a-axis data; the new values are

$$q = 3087.2 \text{ or } -764 \text{ cm}^{-1}.$$

Incorporation of the nonlinear parameters and the new q values has further improved the good agreement obtained earlier for shock loading along the c and a axis. Hence, the same is used for calculating the response for shock loading along the r axis.

IV. UNIAXIAL STRAIN ALONG r AXIS

The orientation of r axis ($1\bar{1}02$) is shown with respect to the crystallographic axes and the local trigonal axes (XYZ) in Fig. 1. If we define the direction of shock propagation (r direction) as z', then x' and y' are in the plane of the shock front. The transformation matrix from the shock propagation direction to the trigonal frame can be written in terms of the Euler angles (ϕ, θ, and ψ).[9] In the present case, $\phi = 0°$, $\psi = 0°$, and θ, the angle between (0001) and ($1\bar{1}02$) direction, is 57.6°. For shock propagation along the r axis, we can write the strain matrix in the primed coordinate system as

$$\begin{bmatrix} 0 & 0 & 0 \\ 0 & 0 & 0 \\ 0 & 0 & e \end{bmatrix}. \quad (18)$$

When transformed to the trigonal frame, the strain matrix has the form

$$\begin{bmatrix} 0 & 0 & 0 \\ 0 & 0.7129e & -0.4524e \\ 0 & -0.4524e & 0.2871e \end{bmatrix}. \quad (19)$$

This strain matrix leads to the following symmetry adapted strains:

$$e(A_1) = e, \quad (20)$$

$$e_{x0}(T_2) = -0.06935\frac{e}{\sqrt{3}}, \quad (21)$$

$$e_{x+}(T_2) = \frac{e}{\sqrt{3}}(0.35645 - i0.3199), \quad (22)$$

$$e_{u+}(E) = \frac{e}{\sqrt{6}}(0.7129 + i1.27958). \quad (23)$$

These symmetry adapted strains lead to

$$\epsilon_+ - \epsilon_+^0 = \Pi[e(A_1)]e(A_1) + \Pi(e_{x0})e_{x0} + \frac{12K_1^2}{A'}|e_{x-}|^2 + \frac{\Delta - \Delta_0}{2}, \tag{24}$$

$$\epsilon_- - \epsilon_-^0 = \Pi[e(A_1)]e(A_1) + \Pi(e_{x0})e_{x0} + \frac{12K_1^2}{A'}|e_{x-}|^2 - \frac{\Delta - \Delta_0}{2}, \tag{25}$$

where

$$\Delta = \Delta(\epsilon_+ - \epsilon_-) = 2\left[\left(\frac{2K}{A'}\right)^2 + 0.15293\left(\frac{2K_1 e}{A'}\right)^2 + \left[\left(-0.29104q + 2.46956\frac{KK_1}{A'}\right)e - 0.04944\frac{K_1^2 e^2}{A'}\right]^2 + \left[\left(0.52239q + 2.21633\frac{KK_1}{A'}\right)e + 0.45611\frac{K_1^2 e^2}{A'}\right]^2\right]^{1/2}. \tag{26}$$

ϵ_+^0 and ϵ_-^0 represent energies corresponding to the ambient positions of R_2 and R_1 lines, respectively, and Δ_0 is the R_1–R_2 splitting at ambient conditions. Using Eqs. (24)–(26), we have calculated the shifts and splitting in Sec. V.

V. EXPERIMENTAL METHOD AND RESULTS

The experimental procedures in the present work were very similar to those used previously for shock loading along the *c* and *a* axis.[1,2,4,5] For the present measurements, 0.2 mm thick disks of ruby crystals were cut from a cylindrical rod (Union Carbide Corp., Cr~1.5%) with the surfaces parallel to the crystal plane with Miller indices $(1\bar{1}02)$. These ruby disks were polished to an optical finish on both sides. The crystal orientation was verified with the help of Laue x-ray diffraction and was found to be within ±1°. All shock experiments were carried out at 77 K using a sample cell design developed earlier.[2,5] Ruby disks were bonded with epoxy (Epon 815) to *a*-cut sapphire disks (3 mm thick and 36 mm diameter, Union Carbide Corp.). The aluminum cell,[2,5] sealed with indium o rings was mounted in the target and aligned with respect to the impactor *a* cut sapphire disk (3 mm thick and 36 mm diameter) with the help of an autocollimator (Keuffel and Esser).

A schematic view of the experimental arrangement is shown in Fig. 2. Light from a cw argon ion laser (514.5 nm, Coherent Innova 90-6), transmitted through an optical fiber (Diaguide STU 400 E-SY), is focused to approximately 1 mm to excite the *R*-line luminescence. The same fiber collects the luminescence and delivers it to the monochromator (Spex 1680, 1200 groove/mm) through a dichroic beam splitter (to separate the luminescence from the incident light). The luminescence spectrum is dispersed in time using a streak camera (Imacon 790), intensified by a microchannel plate (ITT F4113, P-11 phosphor), and recorded using an optical multichannel analyzer (EG&G OMA II with CCD detector). The spectral resolution of the recording system is ~0.4 Å/pixel and spectral calibration is performed just before each experiment. The time resolved spectra were recorded at a 45 ns interval for a total time of 1.6 μs. Sample heating is avoided using a shutter which opens 10–20 ms prior to recording the spectra.

Shock waves were generated by impacting the sample with an *a*-cut sapphire impactor mounted on a projectile. A single stage gas gun[10] was used to accelerate the projectile to the desired velocities; projectile velocity was measured just prior to the impact. All of the ruby disks have a large diam-

TABLE I. Summary of experiments.

Experiment No.	Particle velocity[a] (mm/μs)	Density compression[b]	Longitudinal stress[b] (kbar)	Measured *R*-line shift (Å). ΔR_1[c]	ΔR_2[c]
1	0.117	0.010	52.5	11.9	11.4
		−0.0106	−51.5	−9.3	−10.4
2	0.129	0.0115	58	14.3	13.2
3	0.15	0.138	68	17.7	16.0
4	0.183	0.016	82.7	20	17.4
5	0.200	0.018	91	22.5	18.3

[a]This is one-half the measured projectile velocity.
[b]Calculation of these values is discussed in Refs. 1 and 4; density compression is defined as $\rho/\rho_0 - 1$.
[c]Experimental precision associated with these measurements is typically ±0.5 Å as discussed in Refs. 1 and 4.

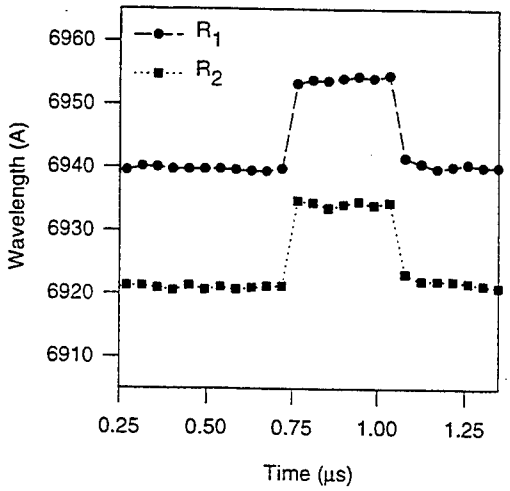

FIG. 3. Shift of the ruby R lines as a function of time for the experiment with a longitudinal compressive stress of 58 kbar. The R_1 data have been offset by +5 Å for visual clarity.

eter to thickness ratio, and the measurements were made in the center of the sample prior to the arrival of edge waves. Five successful uniaxial strain experiments were carried out and these are summarized in Table I. Tensile strain is generated in the shock experiments through the interaction of rarefaction waves as described in Ref. 5. Due to the fact that sapphire is mechanically almost isotropic,[4] it is reasonable to assume that the shock response along r and a axis is the same. Furthermore, the shock response of sapphire at 77 K is the same as at room temperature.[2] Hence, the mechanical quantities listed in Table I can be calculated as before[1,4,5] using the sapphire Hugoniot[11] and the jump conditions.[12]

The time-resolved variation of the positions of the R lines is shown in Fig. 3 for a peak compressive stress of 58 kbar. The data for the R_1 line have been offset vertically by 5 Å for visual clarity. The jump in the R-line positions due to shock wave arrival at the ruby disk is clearly visible. Within the experimental precision (~0.5 Å), the R lines shift back to their original positions upon unloading. A discussion of the experimental precision may be seen in Refs. 1 and 4. The data in Fig. 3 are typical of R-line shifts in the elastic range and are similar to those observed for shock propagation along the c and a axis.[1,4,5] The blue shift associated with tension is qualitatively similar to that shown in Fig. 3 of Ref. 5.

During the present work, we determined that the elastic limit for shock propagation along the r axis was considerably smaller (~65 kbar) than that observed for shock propagation along the c and a axis (the HEL exceeds 125 kbar for these two orientations). This observation, initially surprising, was confirmed independently by our quartz gauge measurements.[13] At stresses above 65 kbar, the shift of the R lines show a time-dependent behavior consisting of a step increase followed by a gradual rounding to the peak value. Since the initial jump will reflect an elastic stress in the ruby, we have used only the shift of the R lines associated with the first jump (Table I) in our present analysis. Issues related to the time-dependent behavior of the R-line shifts will be addressed at a later date.

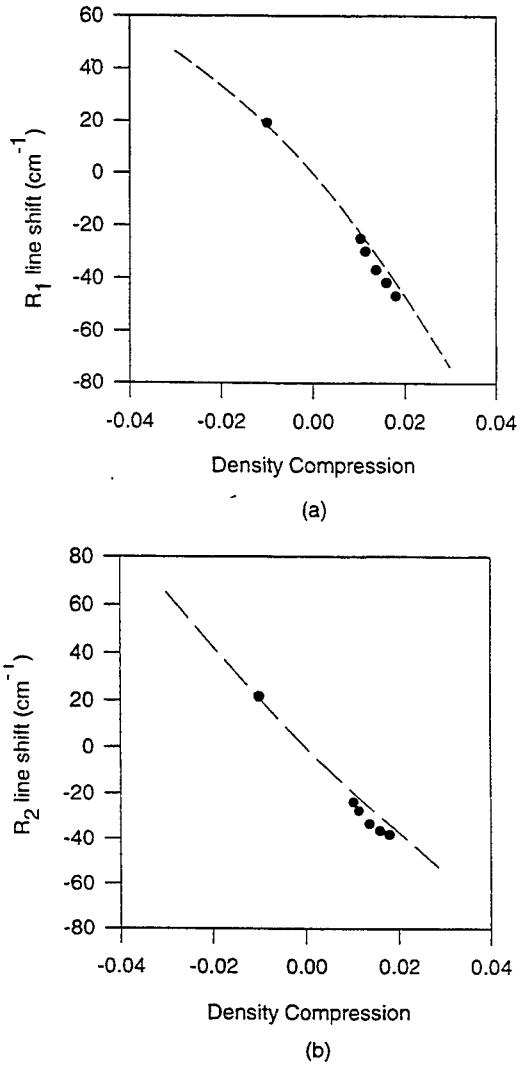

FIG. 4. (a) Comparison of the observed shift of the R_1 line with the theoretical predictions (dashed line). (b) Comparison of the observed shift of the R_2 line with the theoretical predictions (dashed line).

VI. DISCUSSION AND CONCLUSIONS

Shifts of the R_1 and R_2 positions (cm^{-1}) associated with uniaxial strain loading along the r axis are plotted as a function of density compression ($\rho/\rho_0 - 1$) in Figs. 4(a) and 4(b), respectively. The compression data and the datum for tension are compared with the theoretical predictions calculated using Eqs. (24) and (25). The good agreement observed in Figs. 4(a) and 4(b) makes a strong case for the validity of our theoretical model.[3,4]

The R_1-R_2 splitting provides a more stringent test for the model predictions and, within experimental precision, good agreement can again be seen in Fig. 5. The present work has also allowed us to determine a unique value for the parameter q. Earlier results for uniaxial strain along the a axis could not distinguish between the two q values: -764 or $3087.2\ cm^{-1}$. The present data deviate systematically from the positive q value and the R_1-R_2 splitting show good agreement only for $q = -764\ cm^{-1}$. In this context we note that for shock propagation along the r direction, $|e_{u+}/e^*_{x-}| = 2.17$ in contrast to $|e_{u+}/e^*_{x-}| = 1/\sqrt{2}$ for shock propagation along the a axis. Therefore, for the same $e(A_1)$, the R_1-R_2

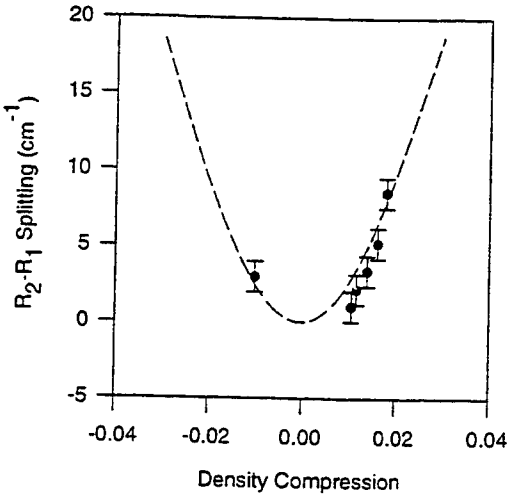

FIG. 5. Comparison of the observed variation of R_1-R_2 splitting data with theoretical calculations (dashed line).

splitting is more sensitive to q in the case of shock propagation along the r axis than along the a axis.

In conclusion, we note that the theoretical formulation presented in Refs. 3 and 4 predicts the shock induced shifts and the splitting of R_1 and R_2 lines of ruby accurately even for uniaxial strain loading along a low symmetry direction. This additional test of the theory lends confidence to the predictive capability of the theoretical model and should encourage its usage under loading conditions where the ruby is subjected to more complex deformations.

In view of the success in predicting the ruby R-line response for shock compression along arbitrary directions, oriented ruby chips can be used to provide a quantitative determination of the stress deviators in diamond anvil cell experiments. These results, in turn, can be used to obtain material strength at very high pressures, and to evaluate the role of nonhydrostaticity on material phenomena at large compressions. R-line measurements along with x-ray data can be used to separate effects due to shear stresses and pressures in DAC measurements.

ACKNOWLEDGMENTS

The assistance of Dr. X. A. Shen and Dr. G. I. Pangilinan with some of the early experiments is sincerely appreciated; the tension experiment reported here was carried out by Dr. Pangilinan. K. Zimmerman and D. Savage are acknowledged for their assistance with the impact experiments. This work was supported primarily by DNA under Contract 001-92-C-0063.

[1] P. D. Horn and Y. M. Gupta, Phys. Rev. B **39**, 973 (1989).
[2] J. A. Burt, Ph.D. thesis, Washington State University, 1989.
[3] S. M. Sharma and Y. M. Gupta, Phys. Rev. B **43**, 879 (1991).
[4] X. A. Shen and Y. M. Gupta, Phys. Rev. B **48**, 2929 (1993).
[5] Y. M. Gupta, P. D. Horn, and J. A. Burt, J. Appl. Phys. **76**, 1784 (1994).
[6] T. S. Duffy, R. J. Hemley, and H. K. Mao, Phys. Rev. Lett. **74**, 1371 (1995).
[7] R. J. Hemley, H. K. Mao, G. Shen, J. Badro, P. Gillet, M. Hanfland, and D. Hausermann, Science **276**, 1242 (1997).
[8] N. Funnamori, T. Yagi, and T. Uchida, J. Appl. Phys. **75**, 4327 (1994).
[9] H. Goldstein, *Classical Mechanics* (Addison-Wesley, Palo Alto, CA, 1964), Chap. 4.
[10] Y. M. Gupta, D. D. Keogh, D. F. Walter, K. C. Dao, D. Henley, and A. Urweider, Rev. Sci. Instrum. **51**, 183 (1980).
[11] L. M. Barker and R. E. Hollenbach, J. Appl. Phys. **41**, 4208 (1970).
[12] G. E. Duvall, in *Physics of High Energy Density* (Academic, New York, 1971), pp. 7–50.
[13] J. K. Hyun and Y. M. Gupta (unpublished).

APPENDIX B
FEASIBILITY OF STIMULATED EMISSION TO MEASURE R-LINE SHIFTS IN SHOCK COMPRESSED RUBY

M. D. Knudson and Y. M. Gupta[a)]
Institute for Shock Physics and Department of Physics, Washington State University, Pullman, Washington 99164-2816

(Received 28 October 1998; accepted for publication 27 January 1999)

In previous studies, ruby *R*-line shifts under shock compression and tension have been measured using the spontaneous luminescence from optically pumped samples. The signal intensities obtained are limited by the short time duration of the experiments in comparison to the long lifetime of the luminescence. We have investigated the use of stimulated emission for measuring *R*-line shifts in shocked ruby crystals. Experiments were performed both at ambient conditions and under shock compression to 6 GPa using an experimental configuration similar to that used for time resolved ruby luminescence measurements in previous shock wave studies. Signal gain due to stimulated emission was observed, with gains ranging from 1.1 to 3.4, in agreement with calculations performed for the particular experimental configuration used. The present results make a good case for incorporating this technique into the measurement of shock induced *R*-line shifts in ruby.
 [S0021-8979(99)07109-1]

I. INTRODUCTION

A comprehensive study of time-resolved *R*-line shifts in ruby crystals subjected to compressive and tensile loading in plate impact experiments has been carried out by Gupta and co-workers.[1–8] The success of the theoretical analysis[4,6,8] in accurately modeling the ruby *R*-line shifts for a variety of loading conditions has prompted the use of ruby as a stress sensor in dynamic loading experiments.[9] Typically, the *R*-line positions are measured by collecting the spontaneous luminescence. However, the signal intensities obtained in shock wave experiments through the use of this method are limited by the rather long lifetime of the ruby luminescence. The typical duration of a shock experiment is on the order of 100 ns–1 μs, while the *R*-line luminescence lifetime is approximately 3 ms.[10] Thus only a very small fraction of the energy stored in the ruby is emitted during the course of the experiment. Further, the energy emitted fluoresces into all angles; only a fraction of this emission is collected and sent to the detection system. The use of stimulated emission to enhance the *R*-line luminescence would overcome both of these limitations. By seeding the emission of the ruby, more of the energy stored in the ruby would be released during the experimental duration, and this energy would be released directionally to permit better coupling to the detection system. Because the strength of the stimulated signal is proportional to the inducing probe signal, one is not limited by the strength of the spontaneous luminescence signal when considering the collection spot diameter or the time resolution in time-resolved experiments.[2] The objective of this work was to investigate the feasibility of using stimulated emission to measure *R*-line shifts in shocked ruby crystals.

In Sec. II we present a brief summary of stimulated emission and describe our calculations performed to determine if stimulated emission could be observed using the experimental configuration used to obtain time-resolved ruby luminescence measurements under shock loading.[1,2,6,7] In Sec. III we summarize the experimental method used, and discuss the results of ambient and shock wave experiments performed to test calculational predictions. Concluding remarks are given in Sec. IV.

II. THEORETICAL BACKGROUND AND CALCULATIONS

In order to realize stimulated emission in ruby, there must exist a population inversion of the Cr^{+3} ions responsible for the *R*-line emissions. The probability of induced absorption or emission is equal.[10] Thus, which of these two processes will dominate depends upon the relative number of ions in the ground and excited states. This is explicitly apparent in the expression[10]

$$\frac{dI_\nu(z)}{dz}=\frac{(N_2-(g_2/g_1)N_1)c^2}{8\pi n^2\nu^2\tau}g(\nu,\nu_{12})I_\nu(z)\equiv\gamma_\nu(z)I_\nu(z), \tag{1}$$

where I_ν is the intensity of the light at frequency ν, z is the spatial coordinate in the direction of light propagation, and γ_ν is called the small signal gain coefficient. N_1 and N_2 and g_1 and g_2 are the population densities and the degeneracy factors of the ground and excited states, respectively; n is the index of refraction of the crystal; τ is the spontaneous lifetime of the transition; and $g(\nu,\nu_{12})$ is a normalized distribution function, centered at frequency ν_{12}, which describes the line shape of the transition between the ground and excited states.

At thermal equilibrium, the ratio of the excited state and ground state populations is given by a Boltzmann distribution, and thus the small signal gain coefficient, γ_ν, is negative. In this situation absorption will dominate, and the in-

a)Electronic mail: shock@wsu.edu

tensity of light at or near the frequency of the transition, denoted by ν_{12}, will be attenuated as it propagates through the crystal. If, on the other hand, the crystal is excited such that there exists a population inversion of the ions, then δ_ν is positive, and the intensity of light at or near the frequency ν_{12} will grow exponentially as it propagates through the crystal; optical gain will occur through the process of stimulated emission.

It should be noted that the derivation of Eq. (1) approximates the active ion as a simple two level system.[10] The Cr^{+3} ion in ruby is not quite a simple two level system. The ions are optically pumped from the ground state to the excited state, a metastable ^2E state, through the broad $^4F_1$ and $^4F_2$ bands; these bands have an extremely short lifetime, with the ions undergoing a nonradiative decay to the metastable ^2E state. Further, the metastable ^2E state consists of two sublevels, the R_1 and R_2 levels. However, the derivation for the simple two level system is still applicable provided that the excited state population density includes only the ions of the sublevel of interest.[11] Since the relaxation time between the sublevels is on the order of a nanosecond or less,[11] the ratio of the population densities of the sublevels is essentially constant and is given by a Boltzmann factor $\Gamma \equiv N_2(R_2)/N_2(R_1) = \exp(\Delta E/k_bT)$, where ΔE is the energy difference between the R_1 and R_2 levels (approximately 29.1 cm^{-1} at ambient conditions).

Given that Γ is essentially a constant, the small signal gain coefficients for ruby can be rewritten in terms of Γ. It is also useful to replace the ground state and excited state population densities, N_1 and N_2, with the excitation ratio $r \equiv N_2/N_{\text{total}}$. Rewriting Eq. (1) or the usual gain equation[10] in terms of these quantities, the small signal gain coefficients for the R_1 and R_2 transition are given by

$$\gamma_{R_1}(\nu) = \frac{N_{\text{total}}[r/(1+\Gamma) - (g_2/g_1)(1-r)]c^2}{8\pi n^2 \nu^2 \tau} \times \frac{\Delta\nu}{2\pi}[[(\nu-\nu_{R_1})^2 + (\Delta\nu/2)^2]^{-1}, \quad (2)$$

and

$$\gamma_{R_2}(\nu) = \frac{N_{\text{total}}[r/(1+\Gamma^{-1}) - (g_2/g_1)(1-r)]c^2}{8\pi n^2 \nu^2 \tau} \times \frac{\Delta\nu}{2\pi}\{(\nu-\nu_{R_2})^2 + [(\Delta\nu/2)]^2\}^{-1}, \quad (3)$$

where $g(\nu, \nu_{12})$ has been replaced by a Lorentz function of width $\Delta\nu$, which accurately describes the line broadening of the ruby transition due predominately to thermal broadening.[11]

For the ruby used in this study, consisting of 0.4 wt% Cr_2O_3, the gain coefficient for both the R_1 and R_2 transitions can be quite high. Using the parameters of ruby with this chromium concentration, the gain coefficients per unit length at the peak of the R_1 and R_2 transitions are

$$\gamma_{R_1} = 2.66(2.07r - 1)/\text{cm (room temp.)}, \quad (4)$$

$$= 9.25(2.14r - 1)/\text{cm (160 K)}, \quad (5)$$

and

$$\gamma_{R_2} = 2.93(1.93r - 1)/\text{cm (room temp.)}. \quad (6)$$

Thus, for excitation ratios near unity the small signal gain coefficients are approximately 2.85/cm and 2.72/cm for the R_1 and R_2 transitions at room temperature, respectively, and approximately 10.55/cm for the R_1 transition at 160 K. The reason for the large increase in the gain coefficient at lower temperatures is due to the temperature dependence of the linewidth of the transition;[11] the lower the temperature, the narrower the linewidth of the transition, and thus the larger gain coefficient.

As seen in Eqs. (4)–(6), the extent of the gain realized for light propagation through the ruby crystal depends upon two factors: (i) the extent of excitation of the ruby, and (ii) the thickness of the ruby crystal through which the light propagates. By pumping the ruby via the green absorption band using a pulsed laser, excitation ratios of near unity can be obtained. However, the thickness of the sample in shock wave experiments must necessarily be small; this is particularly true in time-resolved experiments, because the temporal resolution depends on the shock wave traversal time through the sample.[2,6] Thus the sample thickness is the limiting factor in whether or not significant gain can be realized in a shock wave experiment. To determine if significant gain could be achieved for the particular experimental configuration used in time-resolved shock wave studies,[2,6] calculations were performed to predict the gain that could be expected for the experimental configuration described in Sec. III.

To estimate the magnitude of the signal gain due to stimulated emission for the particular experimental arrangement of interest, the following procedure was carried out. For a given pump beam energy, the flux of the pump beam at a distance z into the sample was approximated by

$$F(z) = F_0\{\exp(-\alpha z) + \exp[-\alpha(2d - z)]\}, \quad (7)$$

where F_0 is the incident flux corrected for reflection losses at the crystal surface, α is the absorption coefficient at the pump wavelength, and d is the sample thickness. The first term in Eq. (7) corresponds to the incident pump beam, while the second term corresponds to the residual pump beam reflected from the aluminum/ruby interface (the other surface). Given an expression for the flux as a function of position in the sample, the excitation ratio as a function of position was determined from the solution to the simplified rate equation[10]

$$r(z) \equiv \frac{N_2(z)}{N_{\text{total}}} = \frac{1 - \exp\{[1 + 1/\sigma_{12}F(z)\tau][-\sigma_{12}F(z)t_{\text{pulse}}]\}}{[1 + 1/\sigma_{12}F(z)\tau]}, \quad (8)$$

where $F(z)$ is given by Eq. (7), σ_{12} is the absorption cross section at the pump wavelength, and t_{pulse} is the duration of the pump beam pulse. The signal gain due to stimulated emission was then determined by numerically integrating

$$\frac{dI_\nu}{dz} = \gamma_\nu(z) I_\nu(z), \quad (9)$$

using Euler's method. We note that the use of the small signal gain coefficient in these calculations is justified; gain

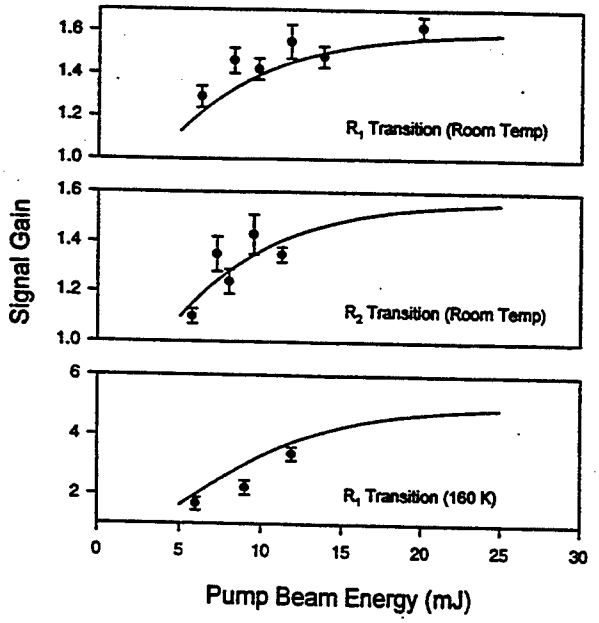

FIG. 1. Signal gain vs pump beam energy. The solid lines indicate the results of the calculations performed for the particular experimental configuration used. The data were taken under ambient pressure conditions.

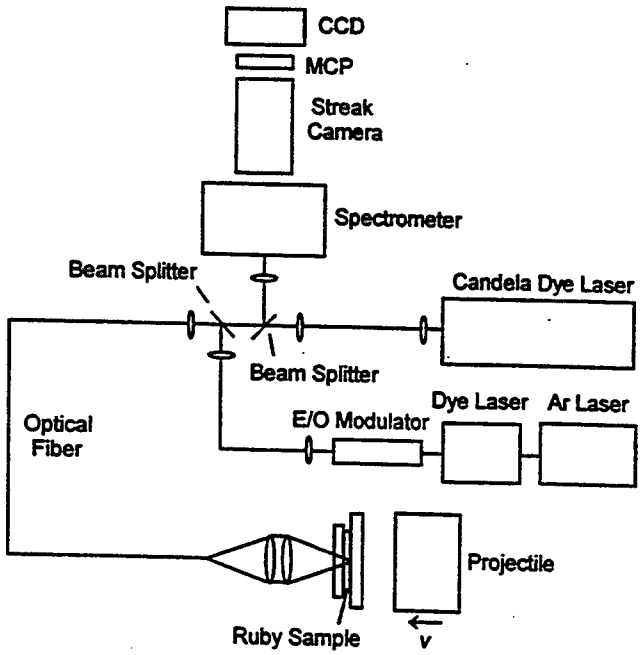

FIG. 2. Schematic of the experimental configuration used to observe stimulated emission under shock compression.

saturation, due to significant depletion of the excited state population,[10] is not an issue in the present experiments. This is because of (i) the efficient pumping of the ruby through the use of a pulsed dye laser resulting in excitation ratios of near unity, (ii) the relatively low intensity of the probe beam which is comparable to the intensity of the spontaneous emission, and (iii) the short time scale of the present experiments with respect to the spontaneous emission lifetime. All three of these factors preclude significant depletion of the excited state population during the time scale of the present experiments.

The results of the calculations performed to determine the signal gain as a function of pump beam energy at the R_1 and R_2 transitions at room temperature, and the R_1 transition at 160 K, are shown in Fig. 1. These calculations were performed at the frequency corresponding to the peak in the R_1 and R_2 transitions for a ruby sample thickness of 800 μm. The asymptotic behavior of the signal gain with the increase in pump beam energy is due to the fact that complete population inversion is approached. Thus for pump beam energies above approximately 20 mJ the gain coefficient is nearly a maximum throughout the crystal and the maximum possible signal gain is achieved. The calculational results suggest that signal gains as large as 1.6 can be obtained at room temperature using experimental configurations typically used in time-resolved shock wave studies.[2,6]

III. EXPERIMENTS AND RESULTS

The experimental configuration considered for the calculations, and used to observe stimulated emission in this study, is shown schematically in Fig. 2. This experimental configuration is similar to that used in previous time-resolved ruby luminescence measurements under shock loading.[1,2,6,7] A 19 mm diam by 800 μm thick, *c*-cut ruby disk (0.4 wt % Cr_2O_3) was epoxied between a 6061-T6 aluminum disk and a *c*-cut sapphire disk. The epoxy bond thicknesses between the disks were measured to be less than 2 μm. A lens assembly, positioned behind the sample, focused the output of an optical fiber to a spot size of approximately 400 μm at the aluminum/ruby interface. This fiber was used to deliver both the output of a pulsed dye laser (Candella SLL 5000), to optically pump the ruby through the green absorption band, and the output of an electro-optic modulated (Con-Optics model 380) continuous wave (cw) dye laser (Coherent CR599 pumped by a Coherent Innova 90 Ar^+ laser), to seed the ruby emission. The aluminum disk was highly polished to provide a reflective surface at the aluminum/ruby interface. The reflective surface allowed for a double pass of the pump beam and probe beam through the ruby sample. Such an arrangement provided a longer path length through the ruby crystal, which resulted in more efficient pumping of the ruby and a larger increase in the signal gain of the probe beam.

The same fiber used to deliver the pump and probe pulses was also used to collect the spontaneous and stimulated emission from the ruby sample. The collected emission was coupled into the detection system using a dichroic beam splitter. The signal was spectrally dispersed by a spectrometer (SPEX 1680, *f*/4, 0.22 m). The output of the spectrometer was then incident on a streak camera (Hadland Photonics, Imacon 790), which provided temporal dispersion. The streak camera output, a two-dimensional distribution of light intensity with wavelength along one axis and time along the other, was intensified with a microchannel plate image intensifier (ITT model F4113), and digitally recorded on a charge coupled device (CCD) (EG&G model 1430P). The CCD image was binned along the time axis into 64 spectra, each separated in time by 32 ns. Details concerning the timing and synchronization in these experiments can be found elsewhere.[1,2,6,7]

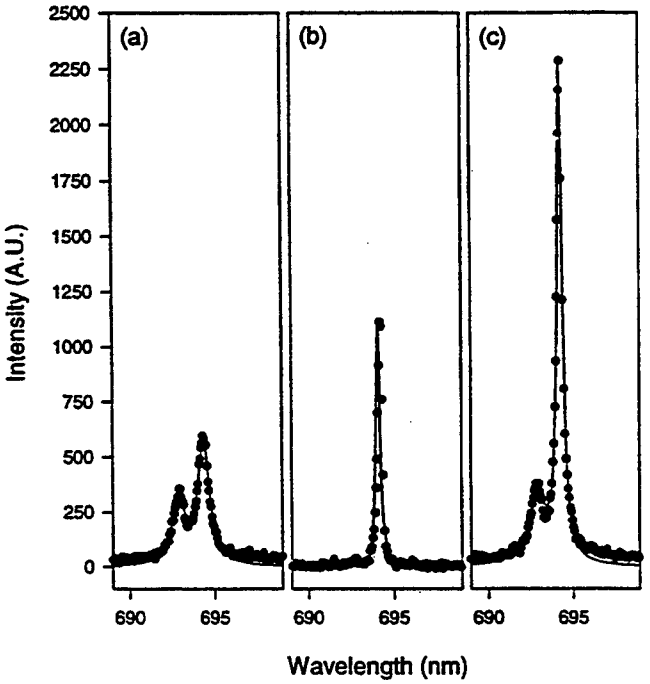

FIG. 3. Spectra obtained to quantify the signal gain: (a) spontaneous signal, corresponding to the spontaneous luminescence, (b) probe signal, corresponding to the cw dye laser probe beam, and (c) induced signal, corresponding to the spontaneous luminescence, stimulated emission, and the probe signal. The solid lines are the fits to the data.

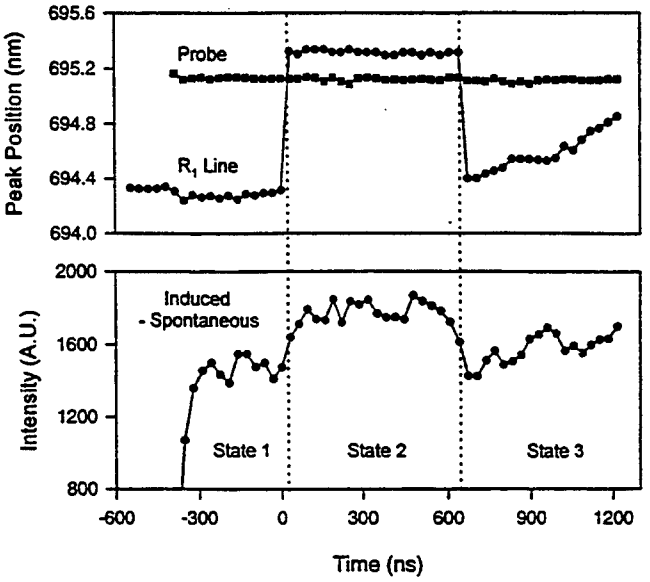

FIG. 4. Results of the shock wave experiment. The peak position of the probe beam and the ruby R_1 line vs time are shown in the top half; the typical measurement precision of our system is ± 0.05 nm. The bottom half shows a plot of the peak counts for the signal of interest (denoted by the difference of the induced and spontaneous emission) vs time.

It should be noted that, ideally, a somewhat broad band, high intensity light source should be used as a probe to stimulate emission. This is because the ruby exhibits two emission lines and, further, these lines shift in wavelength under compression. However, at the time of this study, a suitable broad band, high intensity light source was not available to us. Thus we used a narrow band cw dye laser as the probe beam in these experiments.

A number of experiments were performed under ambient conditions in order to test the predictions of the calculations described in Sec. II. Care was taken to remove the spontaneous emission contribution to the stimulated emission signal in determining the observed gain from the experimental data. To quantify the signal gain the following procedure was followed. At a given pump beam energy, three spectra were taken: (i) the spontaneous signal, corresponding to the spontaneous luminescence from the ruby crystal obtained by pulsing the pump beam with the probe beam off, (ii) the probe signal, corresponding to the cw dye laser probe beam obtained with the probe beam on but not pulsing the pump beam, and (iii) a signal which will be called the induced signal, corresponding to both the spontaneous luminescence and the stimulated emission from the ruby crystal along with the cw dye laser probe beam obtained by pulsing the pump beam with the probe beam on. Each of the spectra, shown in Figs. 3(a)–3(c), were then fitted to Lorentzian peaks, and the remainder of the analysis was done using the peak values of the Lorentzians. The gain for each spectrum was determined by calculating the ratio (induced −spontaneous)/probe. This exercise was performed for each of the 32 ns time-resolved spectra. The signal gain and uncertainty in the signal gain were then determined from the average and standard deviations of the values determined for each spectrum, respectively. The results of experiments performed at the R_1 and R_2 transitions at ambient pressure are displayed in Fig. 1, along with the results of the calculations. The observed gain ranged from 1.1 to 3.4, in reasonable agreement with the calculated results.

To observe stimulated emission under shock compression, a shock wave experiment was performed using the experimental configuration described above. As mentioned earlier, ideally a somewhat broad band light source should be used as a probe to stimulate the emission because the ruby R lines shift under shock compression. At the time of this study, since no such light source was available to us, it complicated the shock experiment. In order to observe stimulated emission under shock compression the dye laser used to seed the ruby emission, with a linewidth of less than 0.1 nm, had to be tuned to the wavelength at which the R_1 line, with a linewidth of approximately 0.5 nm, was expected to shift to under compression. This was made possible, given the theoretical model[4,6] developed to predict the ruby R-line shifts for arbitrary loading conditions.

A plane shock wave was generated by impacting the sample with a 6061-T6 aluminum projectile accelerated by a light gas gun[12] to a velocity of 0.51 km/s. The stress reached in the ruby sample, determined from the measured projectile velocity and the known shock response of the various materials,[2,6,7,13] was approximately 6 GPa. Based on the theoretical model,[4,6] the expected redshift in the R_1 line was 0.94 nm.

The results of the shock experiment are shown in Fig. 4. Plotted in the top half of Fig. 4 are the peak positions versus time of the probe beam and the ruby R_1 line. Figure 4 can be divided into three distinct regions: (1) the pre-shock state, in which the ruby was at ambient conditions, (2) the shocked

state, in which the ruby was held at approximately 6 GPa, and (3) the postshock state, which began at the arrival of the rarefaction wave and included the arrival of the edge waves. As can be seen, the peak position of the R_1 line shifted slightly past the peak position of the probe beam in the shocked state. This was due to two factors: (i) the probe beam wavelength was tuned to a slightly shorter wavelength than desired, and (ii) the actual projectile velocity was slightly higher than was desired (in gas gun experiments, projectile velocities can only be predicted to within a few percent), which resulted in a slightly larger shift in the R_1 line than anticipated. Upon arrival of the rarefaction wave, the R_1 line returned nearly to the ambient position, and slowly approached the probe beam position as edge waves reached the probed region of the sample.

The bottom half of Fig. 4 shows the peak counts for the signal of interest (the difference between the induced and spontaneous signals) versus time. Figure 4 very nicely illustrates the effect of the R_1 line position on the stimulated emission signal. Not only was there stimulated emission in the region corresponding to the shocked state, but there was also a gradual increase in stimulated emission as the R_1 line slowly approached the probe position in region 3.

A procedure similar to that used in the ambient experiments was followed to quantify the gain observed in the shocked state. The observed gain was measured to be 1.23 ± 0.04. Had the R_1 line shifted to the wavelength position of the probe beam exactly, the expected signal gain for this experiment would have been approximately 1.5. However, in the shocked state the peak positions of the R_1 line and the probe signal were separated by approximately 0.2 nm. Because the gain curve follows the line shape function of the R_1 transition, the 0.2 nm separation resulted in a gain coefficient which was reduced from the peak value. Taking into account this reduced coefficient, the expected increase in the probe signal was calculated to be 1.27, which is in good agreement with the observed signal gain.

We note that an optimal test of the calculational predictions would be a shock experiment performed at low temperatures. The expected signal gain due to the narrower linewidth at low temperatures should be nearly a factor of 5. Shock experiments on ruby cooled to 77 K have been performed previously.[14] However, the difficulty in overlapping the peak positions of the cw dye laser (linewidth of less than 0.1 nm) and the shifted R_1 line emission at 77 K (linewidth of approximately 0.1 nm) in a shock experiment has prevented such an experiment from being performed. A broad band, high intensity light source is required for the 77 K experiment.

IV. CONCLUDING REMARKS

We have observed stimulated emission in ruby using an experimental configuration similar to that used previously[1,2,6,7] to obtain time-resolved R-line luminescence measurements under shock compression and tension. At ambient conditions signal gains ranging from 1.1 to 3.4 were observed, in good agreement with calculations performed for the particular experimental arrangement used. Signal gain of 1.24 ± 0.03, in agreement with the predicted signal gain of 1.27, was also observed in a plate impact shock experiment. These results make a good case for incorporating this technique into the measurement of R-line shifts in shocked ruby, and in particular in the development of ruby sensors for stress measurements.[9] The advantage of using stimulated emission is that the stimulated signal is proportional to the inducing probe signal, and thus the signal strength is determined by the probe strength.

However, for this technique to be practical for shock wave experiments, a somewhat broad band, high intensity light source must be identified and incorporated into the experiments. We note that a possible light source is fluorescence from a dye solution excited by a pulsed laser. Such a light source has recently been used in picosecond time-resolved absorption/transmission measurements in shock wave experiments.[15] The technique uses a pulsed Nd:YAG laser to obtain intense broad band emission (approximately 100 nm spectral coverage) from a mixture of coumarin 500 and DCM laser dyes. A similar technique using a pulsed laser with a pulse width on the order of a few μs and laser dyes which fluoresce near 700 nm may serve as a suitable broad band source for stimulated emission experiments. Future experimental work will investigate the use of such a light source.

ACKNOWLEDGMENTS

The authors would like to thank Kurt Zimmerman and Dave Savage for their assistance in performing the impact experiments. One of the authors (Y.M.G.) would like to thank Dr. X. A. Shen for discussions regarding hole-burning measurements which served as a precursor to the work presented here. This work was supported mainly by DNA Contract No. 001-92C0063 and, in part, by DOE Grant No. DEFG03975SF21388.

[1] P. D. Horn and Y. M. Gupta, Appl. Phys. Lett. **49**, 856 (1986).
[2] P. D. Horn and Y. M. Gupta, Phys. Rev. B **39**, 973 (1989).
[3] S. M. Sharma and Y. M. Gupta, Phys. Rev. B **40**, 3329 (1989).
[4] S. M. Sharma and Y. M. Gupta, Phys. Rev. B **43**, 879 (1991).
[5] Y. M. Gupta and X. A. Shen, Appl. Phys. Lett. **58**, 583 (1991).
[6] X. A. Shen and Y. M. Gupta, Phys. Rev. B **48**, 2929 (1993).
[7] Y. M. Gupta, P. D. Horn, and J. A. Burt, J. Appl. Phys. **76**, 1784 (1994).
[8] J. K. Hyun, S. M. Sharma, and Y. M. Gupta, J. Appl. Phys. **84**, 1947 (1998).
[9] Y. M. Gupta, Bull. Am. Phys. Soc. **40**, 1376 (1995); Y. M. Gupta, K. A. Zimmerman, and C. P. Constantinou (unpublished).
[10] A. Yariv, *Quantum Electronics*, 2nd ed. (Wiley, New York, 1975).
[11] W. Koechner, *Solid State Laser Engineering* (Springer, New York, 1976).
[12] Y. M. Gupta, D. D. Kough, D. F. Walker, K. C. Dao, D. Henley, and A. Urweider, Rev. Sci. Instrum. **51**, 183 (1980).
[13] R. Feng and Y. M. Gupta, Internal Report, Institute for Shock Physics, Washington State University, Pullman, WA, 1996 (unpublished).
[14] J. A. Burt and Y. M. Gupta, in *Shock Waves in Condensed Matter–1987*, edited by S. C. Schmidt and N. C. Holmes (Elsevier, New York, 1988), p. 695.
[15] M. D. Knudson, Ph.D. thesis, Washington State University, 1998 (unpublished); M. D. Knudson and Y. M. Gupta, Phys. Rev. Lett. **81**, 2938 (1998).

APPENDIX C
DEVELOPMENT AND USE OF MINIATURE RUBY SENSORS IN PLATE IMPACT EXPERIMENTS

Y.M. Gupta, K.A. Zimmerman, A. Brown and C.P. Constantinou
Institute for Shock Physics
and Department of Physics
Washington State University
Pullman, Washington 99164-2816

I. INTRODUCTION

The development and use of miniature ruby sensors in shock wave (or dynamic loading) experiments was the principal objective of this project. This development is the culmination of a comprehensive research effort[1-6] designed to develop purely optical stress sensors for use in high stress and high strain-rate loading environments. As indicated in the main part of the report, the successful development of such sensors will have broad applicability in many DOD programs involving rapid impulsive loading.

In this Appendix, we describe the experimental methods and results related to the development of miniature ruby sensors and their use in a wide variety of sample materials (metals, polymers, ceramics, and geologic solids) subjected to plate impact loading. The use of plate impact loading ensures a state of uniaxial strain in the samples. This loading condition and the particular choice of sample materials (aluminum, PMMA, polycrystalline aluminum oxide, fused silica, and carrara marble) permit an accurate determination of longitudinal stresses in these materials from published shock wave studies. For two of these materials (fused silica and alumina), the complete stress state is known for uniaxial strain loading over the stress range of interest.[7-9] For 6061-T6 aluminum, reasonable estimates can be made regarding the complete stress state.[10] For PMMA[7] and carrara marble[11], it is difficult to determine the mean stress in the shocked state because of complexities in the material response.

In the development and use of a new type of an in-situ sensor, it is important that the stress state in the sample materials be well characterized as much as possible. Because the stress state in the sensor will be different from the stress state in the material (due to differences in their mechanical properties), a good understanding of the stress state in the sample is necessary to understand and validate the sensor response.

II. EXPERIMENTAL METHOD

A. Overall Configuration and Approach

The experimental configuration used in the present work is shown schematically in Figure 1. Because most aspects of the optical components and the recording instrumentation have been described elsewhere,[4-6] only a brief summary is presented here. A 6.35 cm bore single stage, light gas gun was used to accelerate projectiles to the desired velocities.[12] Either 6061 T6 aluminum or OFHC copper discs were mounted on the projectiles and impacted onto the samples to obtain the desired stresses in the various experiments; shock response of these materials has been well characterized.

Miniature ruby sensors ranging from 400 μm to 1000 μm in diameter and 250 μm in thickness were cut from polished ruby discs (19 mm diameter by 250 μm thick); the normal to the discs was oriented along the crystal c- or a-axis. Thus, all of the ruby chips used in our work had a well defined orientation. Each ruby chip was carefully examined to ensure that no cracks or blemishes were present and to ensure well polished surfaces and smooth edges. The miniature ruby sensors were bonded to either a fused silica optical fiber that had a 400 μm diameter fused silica core and 50 μm thick fused silica cladding or sapphire fibers with diameters ranging from 400 μm to 1000 μm and no cladding. Prior to mounting the chip, the fiber was polished to ensure that the tip was flat and perpendicular to the fiber axis. The measured epoxy bond thickness between the ruby sensor and the fiber was typically ≤5 μm.

In all of the experiments conducted, the target (or sample) consisted of two parts: a thin cylindrical disc (35-38 mm in diameter and 0.8-1.5 mm thick) and a thick cylindrical disc (typically 16-19 mm thick) of the same material as the front buffer. The choice of the buffer disc and the various sizes cited here were a matter of convenience for sample assembly. All of these can be changed as needed for a given application. In the thicker disc, a suitable hole (20-50 μm larger than the optical fiber diameter) was drilled perpendicular to the impact face to embed the ruby gauge (ruby and fiber assembly) in the target. The ruby gauge was mounted in the target such that the sensor was flush with the impact side of the thicker disc. At this point in our initial experiments, the thin buffer disc was carefully bonded to the thicker disc. In later experiments, the ruby sensor face was first plated with a reflective aluminum or silver layer to reduce the required pump energy and to enhance signal collection prior to bonding the front buffer.

In our experiments, either a CW argon ion laser operating at 514.5 nm or a flashlamp pumped dye laser (~ 3 μs pulse width) tuned to 514.5 nm was used to pump the ruby sensor. The use of a pulsed laser permits more efficient pumping of the ruby sensor. We note that the choice of 514.5 nm light was a matter of convenience. The two main absorption bands of ruby are broad and centered at ~400 nm and ~550 nm. Thus, a broad range of wavelengths could be used to efficiently pump the ruby. The use of a pulsed source coupled with the reflective coating yielded a significant improvement in the signal to noise ratio. A single optical fiber, as shown in Figure 1, was used to deliver the excitation light (514.5 nm) to the sensor and the sensor luminescence to the detection equipment.

At the detection system, the luminescence signal was separated from the reflected excitation light using a dichroic beam splitter. A double spectrograph was used to spectrally disperse the signal followed by a streak camera to provide temporal dispersion. The two-dimensional streak image was intensified using an image intensifier and lens coupled to a CCD array. A multichannel analyzer was used to store the image and display it as intensity vs. wavelength vs. time. For three experiments, a 0.5 meter single spectrograph was used instead of the double spectrograph to obtain better spectral resolution.

The time resolution of the detection system was set between 50-110 ns per spectrum depending on the particular measurement. This time resolution was chosen to give an adequate number of spectra at peak pressure as well as permit a long recording duration. The limiting time resolution of the gauge is determined by the sensor dimensions. For the sensors used in these measurements, the limiting resolution was approximately 50-60 ns. This value is defined by the shock wave propagation times through the ruby thickness and lateral dimensions (the shock wave velocity in ruby is approximately 11 mm/μs at these stresses). Because the gauge perturbs the stress distribution in the target material, the time for the gauge to come to equilibrium is in general longer than the resolution of the sensor itself. We emphasize that considerable flexibility exists for both the time resolution and time duration, and different values can be obtained by a suitable choice of sensor sizes, optical fibers, and detection equipment settings.

Each spectrum was calibrated to convert pixel numbers to wavelengths. This was

accomplished by recording ruby R-lines (R_1 = 6943Å and R_2 = 6929Å) for five different spectrometer settings. The R-line peaks were fit to two Lorentzian functions and the peak position recorded. The five sets of pixel number and spectrometer setting were fit to a line that typically gave a dispersion of 0.6 Å/pixel at the CCD.

Two points need to be emphasized about the above method. The final procedure that was developed was the culmination of a long effort (more than a year) in which we had to learn how to carry out each of the operations properly. Even now, the gauge assembly is quite time intensive and requires considerable care to ensure proper fabrication.

We note that only the miniature ruby disc, and not the fiber, acts as the stress sensor in our work. While the presence of the fiber can alter the dynamic stress distribution in and around the chip (the inclusion problem), its sole purpose is to transmit the light to and from the ruby sensor. Since the completion of this work, we have examined the use of fibers and chips of both smaller and larger sizes.

III. RESULTS AND DISCUSSION

A. Preliminary Measurements

Preliminary measurements were made in 6061 T6 aluminum, OFHC copper, carrara marble, and alumina (Vistal) with peak longitudinal stresses ranging between 40–120 kbar. As indicated earlier, the stresses reported here have been calculated from existing material models and correspond to the stresses in the material subjected to uniaxial strain (in the absence of the gauge).

These preliminary experiments were conducted to determine the feasibility of embedding miniature ruby sensors and to establish a working experimental procedure. Initial ruby sensors were ultrasonically ground to 1 mm diameter. In subsequent experiments, the ruby sensors were laser cut from polished disks to yield more uniform and accurate dimensions with fewer defects. The early measurements also explored the use of lens coupling, direct fiber coupling, using different types of optical fibers, and verification that the epoxy used to bond the sensor and fiber remained transparent at high stresses. In general, the signal quality of these preliminary measurements was poor as compared with more recent measurements. However, the information gathered in these early measurements was central to the development of higher quality

gauges and for obtaining a better signal to noise ratio.

A summary of the measurements performed, after the development of a satisfactory experimental procedure, is given in Table I. Experiments 1-6 represent preliminary measurements. The target materials include 6061-T6 aluminum (aluminum), carrara marble, and Vistal (polycrystalline Al_2O_3) with longitudinal stresses ranging from 40 kbar to 80 kbar. 6061 T6 aluminum was chosen because of a well characterized shock response, ease of machining, and the good impedance match to the embedded fused silica optical fiber. To examine the feasibility of ruby measurements in non-metallic targets, we carried out one experiment with a carrara marble target (40.8 kbar) and one successful measurement with a Vistal target (80.6 kbar). Carrara marble undergoes elastic-plastic deformation and a phase change, and its shock response has been examined carefully by Aidun and Gupta.[11] Vistal is mechanically very similar to sapphire and should minimize the perturbations to the stress field due to the presence of the gauge.

Figure 2a shows typical spectra from a preliminary experiment with a ruby gauge embedded in aluminum and shock loaded to a peak longitudinal stress of 54 kbar. For times less than t = 0 (before the shock wave reaches the sensor), ambient positions of the R-lines are observable. The spectra at time t = 0 has spectral information from both the ambient state and the shocked state. At times greater than t = 0 and less than 2.7 μs, the R-lines are red-shifted due to the applied stress. For times greater than 2.7 μs, there is a broad background increase across the spectral window, the observable R-line intensities decrease dramatically, and the R-lines begin to blue-shift toward the ambient position. The broad background increase is likely due to the fracture of the optical fiber when the shock wave gets to the rear surface of the target. The blue shift is caused by a lateral release wave due to the finite lateral dimensions of the sample. Release waves from the back of the impactor and back of the sample do not arrive at the sensor for ~4 μs and ~6 μs respectively.

There is a substantial decrease in the R-line intensities after the shock wave reaches the sensor. Because all the required information is contained in the spectral shift of the R-lines, the change in intensity does not appreciably affect the results. As compared to more recent measurements, the intensity decrease in the preliminary measurements was more pronounced and, in general, the time duration of the signal at

the shocked state was shorter.

Reference data were taken just prior to the shock measurement. Spectra in both the reference and shocked states were fit to the sum of two Lorentzian functions and a constant background to obtain the R-line peak positions, intensities, and full width at half maximum (FWHM). The results of these fits are shown in Figure 2b as R-line shifts vs. time. As has been noted previously,[4] the R_2 line is only sensitive to the mean stress in the ruby, and the $R_1 - R_2$ splitting is a measure of the stress difference. Because aluminum has a low strength, we expect the R_1 and R_2 line shifts to be nearly equal. From Figure 2b, the shift for both the R-lines are nearly the same for the duration of the measurement. In fact, experiments 1-4 in Table I show that the R- line shifts are nearly equal (within the experimental precision) for all the initial measurements.

The measurement made with a carrara marble target (Table I, experiment 5) was to determine if the ruby gauge could be used in materials other than metals. The results showed higher than normal error bars due to an error in the acquired calibration spectra. However, the data were of good quality for 5.7 μs after the shock wave reached the sensor. The R-line shifts were nearly equal, indicating comparable lateral and longitudinal stresses in the sensor. Because the shock response of the marble is complicated,[11] we did not attempt to analyze the data further. However, the positive results showed the applicability of the sensor to a wider range of materials.

To determine if the gauge configuration in the present work gave a similar output as past measurements,[2-5] using large ruby discs sandwiched between two sapphire windows, we mounted a c-axis ruby sensor to the tip of a c-axis sapphire fiber and embedded the assembly in Vistal (Table I, experiment 6). In this measurement the optical fiber broke at the back of the target before the experiment was conducted. The protruding portion of the fiber was polished and the gauge signal was acquired from the fiber using lens coupling. The target was shock loaded to 80 kbar and R-lines were recorded for 1.8 μs at 50 ns resolution. The signals were of good quality and the shifts recorded matched the earlier c-axis ruby measurements reasonably well[2]. This was the first measurement where a change in the R-line splitting was observed. The success of this measurement showed that the gauge could provide data up to 80 kbar peak stress in the target and that the measured R-line shifts were consistent with earlier results.

B. Recent Measurements

After a working gauge configuration was developed, an effort was undertaken to measure the gauge response in several well defined experiments. Three materials were chosen for these measurements; 6061 T6 aluminum, Rohn & Haas plexiglass II UVA, and Dynasil 1000 fused silica. As indicated earlier, the shock wave response of these materials has been well characterized in previous studies.[7,8,10,13] Hence, the gauge response can be examined in terms of the known sample response. Additionally, these three materials have a considerably different response under shock wave compression. The ten experiments performed are summarized in Table I. The longitudinal stress values listed correspond to uniaxial strain loading in the sample and reflect the values in the absence of the gauge. Mean stress values are listed only for Vistal, fused silica, and aluminum samples; for PMMA, we have listed the mean stress below the HEL (approx. 7.6 kbar).[13] Mean stress values have been provided only when we can determine them with reasonable confidence. Except for aluminum, these values correspond to an elastically compressed state. For aluminum, the mean stress values were determined from an elastic-plastic, strain-hardening material response.[10]

A total of 5 measurements were made in aluminum with peak longitudinal stresses in the target ranging between 21-61 kbar. Data from a typical aluminum measurement are shown in Figure 3. The aluminum target was shocked to 40 kbar with spectra recorded every 100 ns. The first twelve spectra (prior to t = 0) show the R-lines at ambient conditions before the shock wave has reached the sensor. The spectrum at time, t = 0 is a superposition of the positions of the R-lines at ambient conditions and in the shocked state; this spectrum is convenient for establishing the arrival of the shock wave at the sensor. The spectrum at t = 0 shows a slight increase in the background which disappears in the following spectrum. This may be due to a small gap between the sensor and the back surface of the front buffer. For the next 1.5 μs, the R-lines red shift while the sample is under uniaxial strain. Beyond 1.5 μs, the spectra blue shift back to the nearly ambient position and then begin to gradually red shift starting at the 3 μs mark. The blue shift following the initial red shift is due to lateral release from the lateral edge of the impactor. The 5 μs recording time is shorter than the time for reflections to arrive from the backside of either the aluminum impactor or the aluminum target. Hence, the temporal changes observed in Figure 3 are entirely due to lateral

disturbances. *This finding leads to an important conclusion: the ruby gauge can be used to obtain data when the sample is subjected to 2-D loading.* Because of the higher signal to noise ratio in these recent experiments, the R-line splitting could be measured with higher resolution. However, as can be seen from Figure 3b and experiments 7-11 in Table I, the R-line splitting is small and cannot be resolved within the precision of the measurements.

Several items are immediately apparent when comparing Figures 2 and 3. Most obvious is the improvement in the signal to noise ratio. This improvement permits more accurate determination of the peak positions. In addition, the R-lines are observable for a longer time; a good signal to noise ratio is maintained even at late times; the signal intensity does not drop as significantly upon the arrival of the shock front at the sensor; and the signal recovers fully when the stress is released.

In addition to the aluminum experiments, several experiments using PMMA samples were performed (Table I, experiments 12- 15) with peak longitudinal stresses ranging from 3 kbar to 20 kbar. Figure 4 shows the fitted results for the R-line peaks in PMMA shocked to 20 kbar. For times less than t = 0, the sensor is at ambient stress. However, the R-line positions show an apparent small shift. This apparent shift was likely caused by a small change in the spectrometer setting just prior to the shock measurement (this inference was verified as a plausible cause through subsequent testing of the system). For the next 3 μs, the R-lines gradually red-shift to higher wavelengths.

The data in Figure 4 are qualitatively in good agreement with the published response[7] for shocked PMMA. Particle velocity measurements, using laser interferometry, show a rapid initial jump followed by a gradual increase to the peak value. This behavior is compatible with the rate dependent response of PMMA.

Between 3 μs and 3.5 μs the R-line positions are nearly constant, followed by a gradual blue shift from a release wave arising from the back of the impactor. Because of the higher impedance of the aluminum impactor, the release wave results only in a partial unloading of the sample. For times greater than 5 μs, the R-line positions are again constant. As can be seen from Figure 4, the R-line splitting was small but measurable. In general, the R-line splitting from the PMMA experiments was measurable (see Table I) indicating that the sensor is subjected to a different

longitudinal and lateral stress (refer to Table I). In all of the measurements where R-line splitting was observed, the splitting disappeared upon release wave arrival. Without a detailed analysis, it is difficult to comment on this finding.

For the lowest stress measurement, the dispersion of the spectrometer was increased to give a 0.3 Å/pixel resolution at the detector. Even with this resolution, the R-line shift was only 5 pixels at peak stress. However, because of the high quality signals, the scatter in the fitted peak positions of sequential spectra was less than 1/6 of a pixel. The result of the 3.0 kbar measurement in shocked PMMA indicates that the ruby gauge can be used with good precision even at very low stresses.

One measurement was made in fused silica at a peak longitudinal stress of 40 kbar. Because the optical fiber material matches the target material in this experiment, the perturbation of the stress field in the target due to the presence of the fiber is minimized. That is, the ruby sensor is embedded in a sample subjected to uniaxial strain loading. Figure 5 shows the fitted peak positions of the R-lines as a function of time. The recording time resolution for this experiment was set to 50 ns per spectra. For times between 0 and 1.1 μs, the sample is under constant uniaxial strain. For about 400 ns after the initial jump, the R-lines gradually blue shift to a constant value with a splitting of 3.4 Å. The 400 ns needed to achieve the constant values of the R-line positions is likely an indication of the stress state in the ruby sensor coming to an equilibrium with the fused silica surroundings. It is interesting to note that the R_2 line position changes more during this time than the R_1 line position. As shown elsewhere,[4] the R_2 line position corresponds to the mean stress in the ruby. Hence, the data in Figure 5 suggest that the mean stress in the ruby takes longer to equilibrate. This is not surprising because, most likely, the lateral stress equilibration in the ruby would take longer than the longitudinal stress equilibration. Between 1.1 to 1.2 μs, the release from the back of the fused silica impactor is observed in the gauge response. At approximately 1.5 μs, the R-lines shift back to nearly ambient positions. The 1 Å residual shift at late times is beyond the experimental precision value and its origin is not understood at this time.

Finally, we point out that the largest R_1-R_2 splitting (in the peak state) shown in Table I was observed in the fused silica. This is in accord with the stress difference obtained from Conner's work[8] and indicated by the stress values shown in Table I.

C. Discussion

The R-line shifts listed in this report have not been converted to stress histories because the procedures for inverting the measured R-line shifts to obtain stresses that would be present in the samples have not been worked out completely. The difficulty is not in relating the R-line shifts to stresses in the ruby. Instead, it is the relationship between the stresses in the sensor and the stresses in the sample that needs to be worked out (the gauge-matrix interaction or the inclusion problem). Such a determination would require 2-D numerical calculations similar to those carried out recently to analyze lateral piezoresistance gauge response under shock wave loading.[14] Work is currently underway to examine inversion of the ruby R-line shifts to obtain sample stresses.

Although the sensor data obtained here have not been inverted from the R-line shifts to stress, some comments based on our earlier work where the ruby crystals were subjected to plane wave loading are in order.[2-5] The R_2 line shift is related directly to the mean stress in the sensor.[4] The R_1 - R_2 splitting is a measure of the stress difference in the sensor.[2-5] Also, we point out that the "forward problem" involving the calculation of the R-line shifts for an assumed sample response can be carried out using 2-D numerical simulations. We have developed the procedures to interface our piezoluminescence model to the 2-D, wave code calculations. Thus, data similar to those reported here can be used to evaluate the dynamic material response using numerical simulations.

To gain some insight into the ruby R-line shifts in the different materials, we have plotted R_1 and R_2 line shifts as a function of peak longitudinal stresses in Figures 6 and 7, respectively. Recall, that longitudinal stresses (corresponding to uniaxial strain loading in the samples) are known quite accurately for all of the materials from previous shock wave studies. While some inferences can be made regarding the ruby R-line response in each of the materials, no general trends are apparent. This is not surprising because of two main factors: the R-line shifts are not expected to be a simple function of the sample longitudinal stress, and the presence of the optical fiber, in general, perturbs the stress field in the sample.

In Figure 8, we plot only the R_2 line shifts as a function of sample mean stress. We have chosen to plot only those measurements for which the sample mean stress can be

determined reasonably well from independent approaches. In contrast to Figures 6 and 7, a consistent trend is quite apparent. The R_2 line shifts correlate quite well with the sample mean stresses. However, caution is warranted for several reasons: most of the data are for aluminum; despite the closeness of the slopes for the two lines shown, there is a constant offset which is not currently understood; in most of these experiments (except for PMMA), the optical fiber was a reasonably good impedance match to the sample material; the Vistal result is somewhat off. We caution against using the dashed line as a calibration curve for using the R_2 line shifts to obtain sample mean stresses. A careful analytic/numerical effort is needed to understand results in Figures 6-8 before a good calibration curve can be established.

Finally, the practical limits for using these gauges are not presently known. The experiments to date have provided good data up to 80 kbar. However, the ruby itself does not yield till 145-150 kbar (c-axis) and 170 kbar (a-axis), and good fluorescence data have been observed to 170 kbar in other configurations. Work is currently underway to extend the stress range of the ruby gauges and to obtain higher time resolution.

IV. CONCLUDING REMARKS

The miniature ruby gauges developed at Washington State University have produced good quality signals in a wide variety of materials shocked from 3 kbar to 80 kbar. The experimental developments reported here show that miniature optical stress sensors can be used successfully to examine the dynamic material response of metals, ceramics, polymers, and geologic solids. The present work constitutes an excellent start and further work needs to be carried out before the experimental developments reported here can be used routinely. Experiments need to be carried out to quantitatively establish the experimental limits including the stress bounds, accuracy, and time resolution.

More importantly, a careful analytic/numerical effort needs to be undertaken to develop accurate procedures to invert the sensor output in a meaningful manner. Numerical solutions, similar to those carried out for piezoresistance gauges,[14] are needed to develop an in depth understanding of the gauge response and to establish procedures to analyze the gauge output.

V. REFERENCES

1. P.D. Horn and Y.M. Gupta, Appl. Phys. Lett. **49**, 856 (1986).
2. P.D. Horn and Y.M. Gupta, Phys. Rev. B **39**, 973 (1989).
3. S.M. Sharma and Y.M. Gupta, Phys. Rev. B **43**, 879 (1991).
4. Y.M. Gupta and X.A. Shen, Appl. Phys. Lett. **58** (6), 583 (1991).
5. X.A. Shen and Y.M. Gupta, Phys. Rev. B **48**, 2929 (1993).
6. Y.M. Gupta, P.D. Horn, and J. A. Burt, J. Appl. Phys. **76** (3), 1784 (1994).
7. L.M. Barker and R.E. Hollerbach, J. Appl. Phys. **41** (10), 4208 (1970).
8. M.P. Conners, M.S. thesis, Washington State University, 1988.
9. Y.M. Gupta, J. Geophys. Res. 88 (B5), 4304 (1983).
10. R. Feng and Y.M. Gupta, "Material Model for 6061-T6 Aluminum for Use in Shock Wave Experiments and Calculations," Institute for Shock Physics Internal Report, 1994.
11. J.B. Aidun and Y.M. Gupta, J. Geophys. Res., Solid Earth Vol. 100, No. B2, 1955, (1995).
12. Y.M. Gupta, et al., Rev. Sci. Instr. **51**, 183 (1980).
13. Y.M. Gupta, J. Appl. Phys. **51**, 5352 (1980).
14. R. Feng, Y.M. Gupta, and M.K.W. Wong, J. Appl. Phys. **82**, 2845 (1997).

Table I. Summary of results for embedded ruby gauge measurements.

Experiment No.	Impactor-Target Material[a]	Impact Velocity (mm/μs)	Peak Matrix Stress[b] (kbar)		Peak R-Line Shift		R1-R2 Splitting (Å)
			Longitudinal	Mean	R_1-line (Å)	R_2-line (Å)	
1	Al - Al	0.526	40.6	38.4	14.90 ± 0.40	14.90 ± 0.30	0.00 ± 0.50
2	Al - Al	0.717	56.2	53.9	20.50 ± 0.70	20.40 ± 0.90	0.10 ± 1.14
3	Al - Al	0.728	57.2	54.8	20.70 ± 0.42	20.40 ± 0.49	0.30 ± 0.65
4	Cu - Al	0.628	70.4	68.1	25.45 ± 0.30	25.15 ± 0.50	0.30 ± 0.60
5[c]	Al - Marble	0.608	40.8	---	11.89 ± 1.13	11.81 ± 1.18	0.08 ± 1.03
6[d]	Al - Vistal	0.685	80.6	43.0	13.11 ± 0.43	15.16 ± 0.44	-2.05 ± 0.61
7	Al - Al	0.267	20.6	18.4	7.41 ± 0.11	7.11 ± 0.19	0.30 ± 0.22
8	Al - Al	0.519	40.1	37.8	14.82 ± 0.12	14.77 ± 0.13	0.05 ± 0.18
9	Al - Al	0.521	40.2	38.0	14.95 ± 0.13	14.84 ± 0.16	0.11 ± 0.21
10[d]	Al - Al	0.527	40.7	38.5	14.77 ± 0.30	14.88 ± 0.34	-0.11 ± 0.45
11	Al - Al	0.776	61.2	58.9	22.92 ± 0.31	22.80 ± 0.27	0.12 ± 0.41
12	PMMA - PMMA	0.170	3.0	1.95	1.55 ± 0.05	1.34 ± 0.06	0.21 ± 0.08
13	PMMA - PMMA	0.395	7.3	5.10	3.56 ± 0.17	3.07 ± 0.14	0.50 ± 0.22
14	Al - PMMA	0.348	10.6	---	6.39 ± 0.21	5.58 ± 0.33	0.81 ± 0.39
15	Al - PMMA	0.636	20.3	---	12.95 ± 0.23	12.39 ± 0.27	0.56 ± 0.35
16	FS – FS	0.683	39.8	17.8	11.27 ± 0.17	7.87 ± 0.15	3.40 ± 0.23

[a]Al = 6061 T6 aluminum, PMMA = Rohn & Haas plexiglass II UVA, FS = Dynasil 1000 fused silica, Cu = OFHC copper, Marble = carrara marble

[b]Calculated peak longitudinal and mean stress correspond to uniaxial strain loading in the sample.

[c]The large error for the shift is in part due to an error in the calibration spectra.

[d]Lens coupling to the ruby sensor.

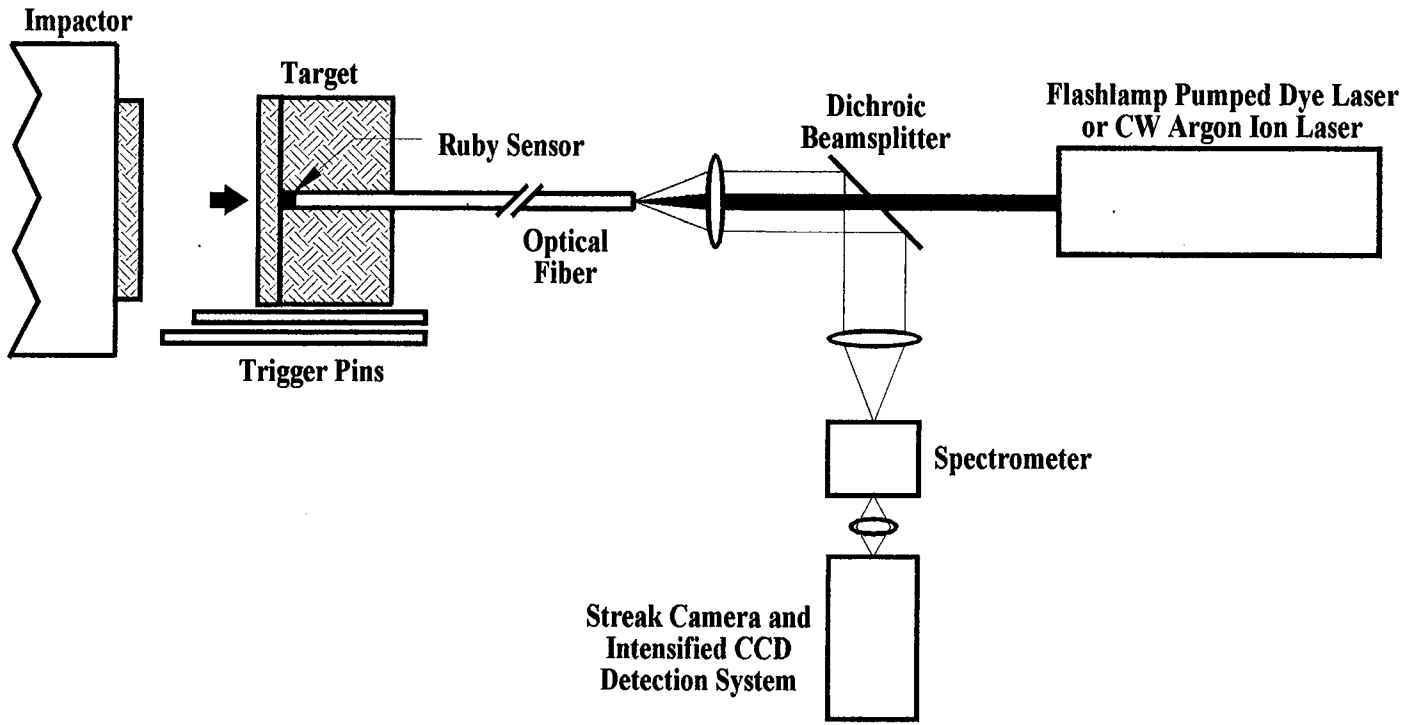

Figure 1: Experimental configuration for obtaining time resolved R-line spectra from an embedded ruby sensor.

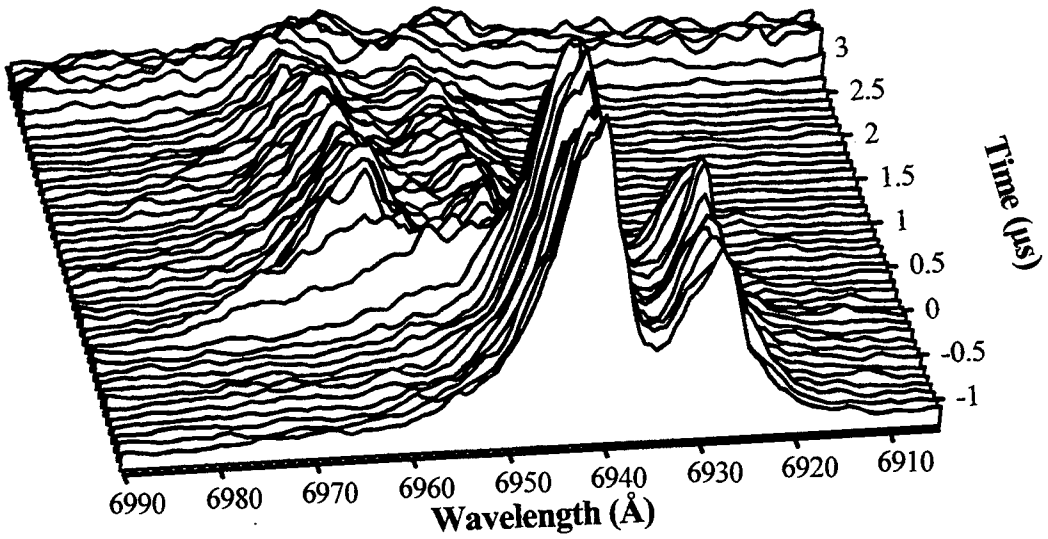

Figure 2a: Time resolved spectra from a preliminary experiment with a ruby gauge embedded in 6061 T6 aluminum shocked to 54 kbar. Sequential spectra were taken every 100 ns. The shock wave reaches the sensor at time t = 0.

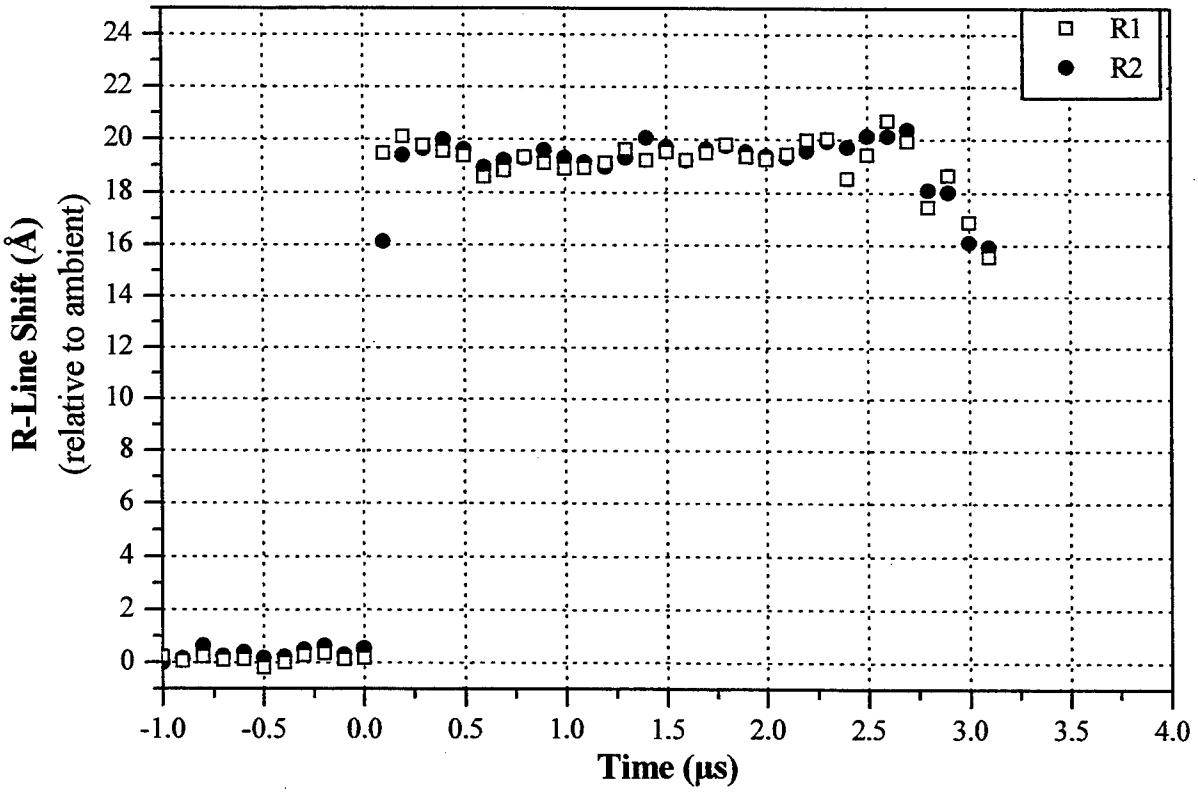

Figure 2b: Fitted peak positions of the ruby R1 and R2 lines as a function of time.

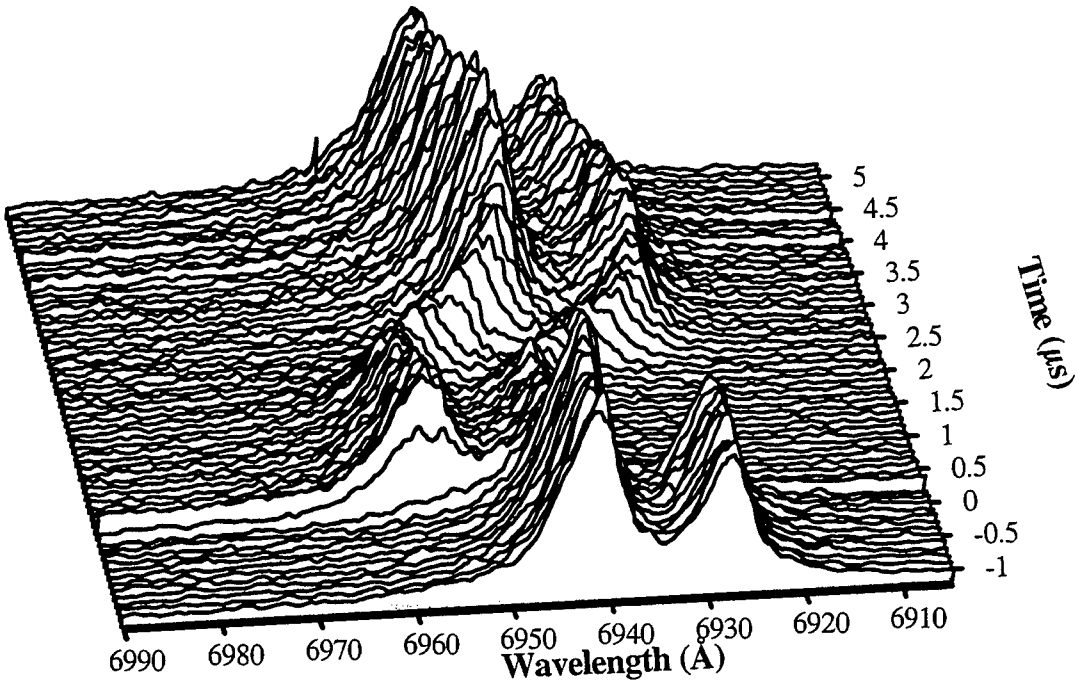

Figure 3a: Time resolved R-line spectra from a ruby gauge embedded in 6061 T6 aluminum shocked to 40 kbar. The shock wave arrives at the gauge at 0 μs followed by a lateral release wave from the edge of the impactor starting at 1.5 μs.

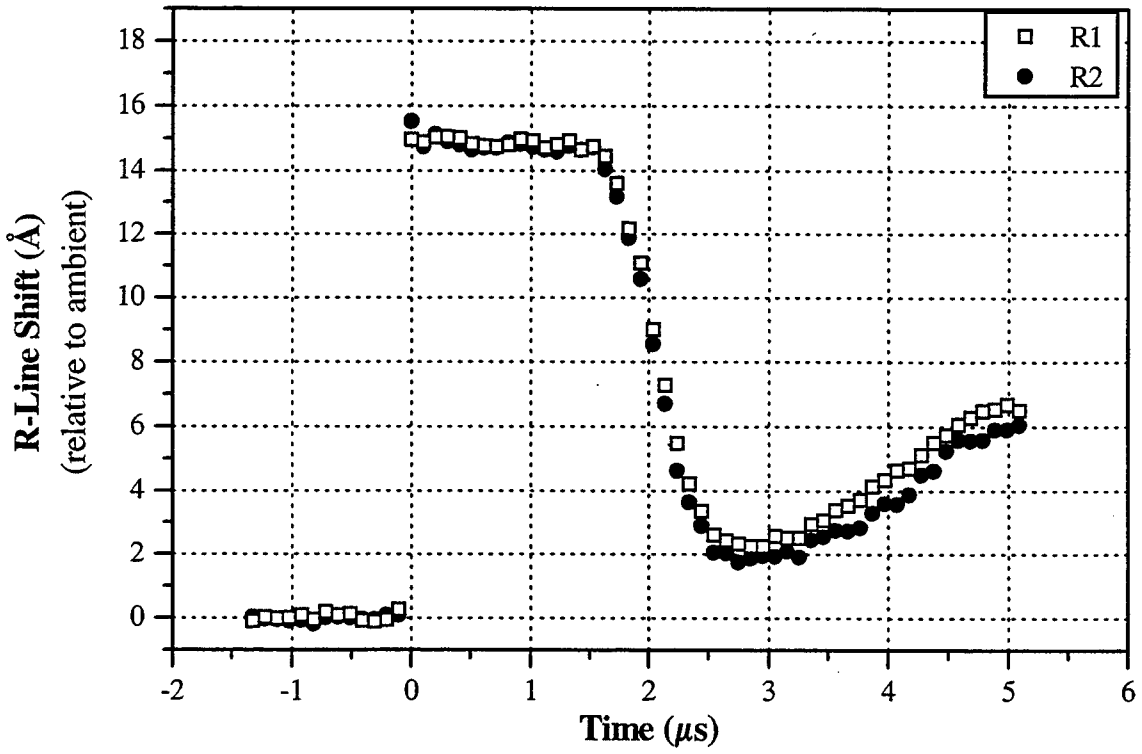

Figure 3b: Fitted peak positions of the ruby R1 and R2 lines as a function of time.

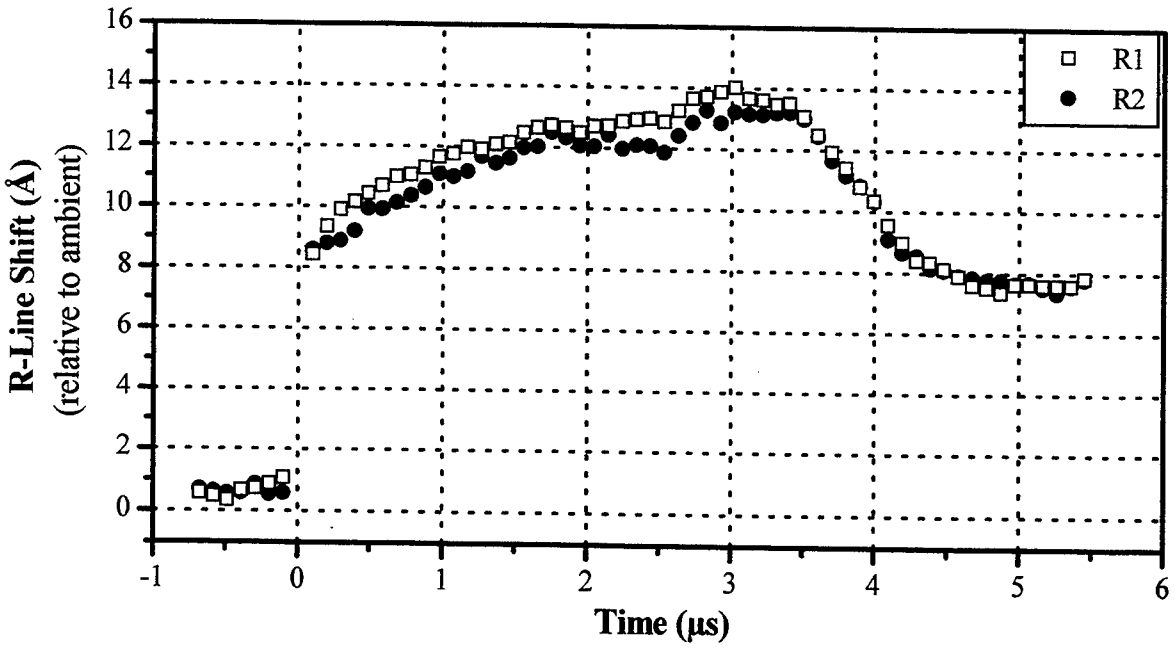

Figure 4: Fitted peak position of the ruby R_1 and R_2 lines as a function of time in PMMA shocked to 20 kbar. The R-line shift gradually increases over 3 μs at which point a release wave from the back of the impactor arrives at the sensor causing a decrease in the shift. Note that the R_2 line shift (related to the mean stress in the sensor) is slightly smaller than the R_1 line during initial loading.

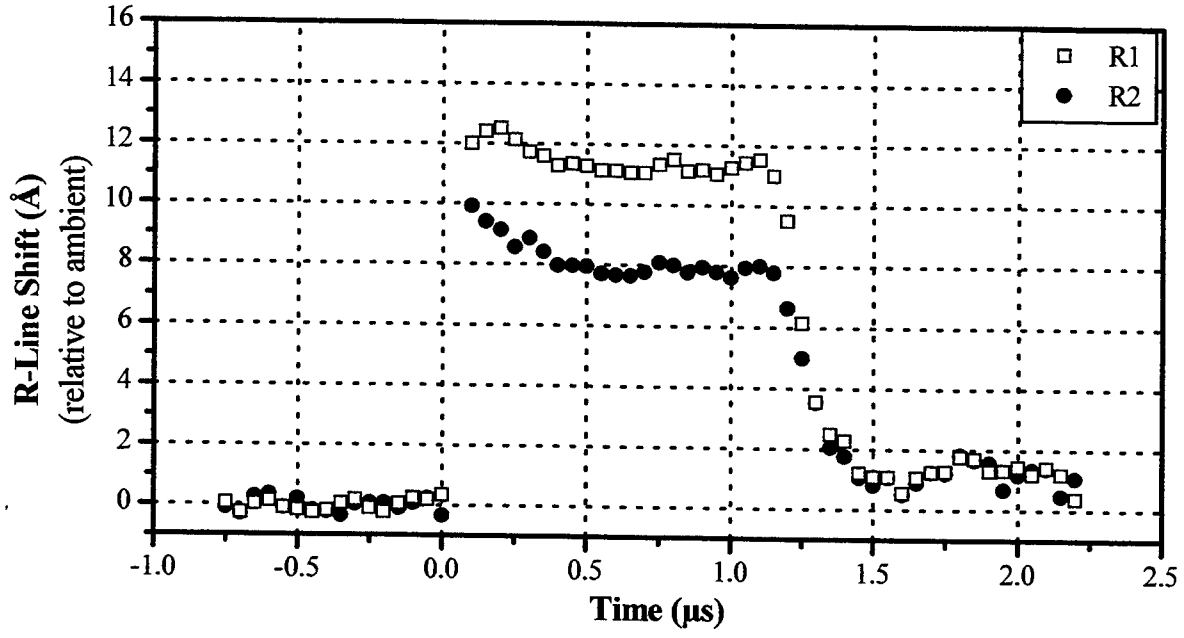

Figure 5: Fitted peak position of the ruby R_1 and R_2 lines as a function of time in fused silica shocked to 40 kbar. Notice the different shifts of the R_1 and R_2 lines which is an indication of the stress difference in the gauge. This phenomena is consistent with the known stress difference in fused silica.

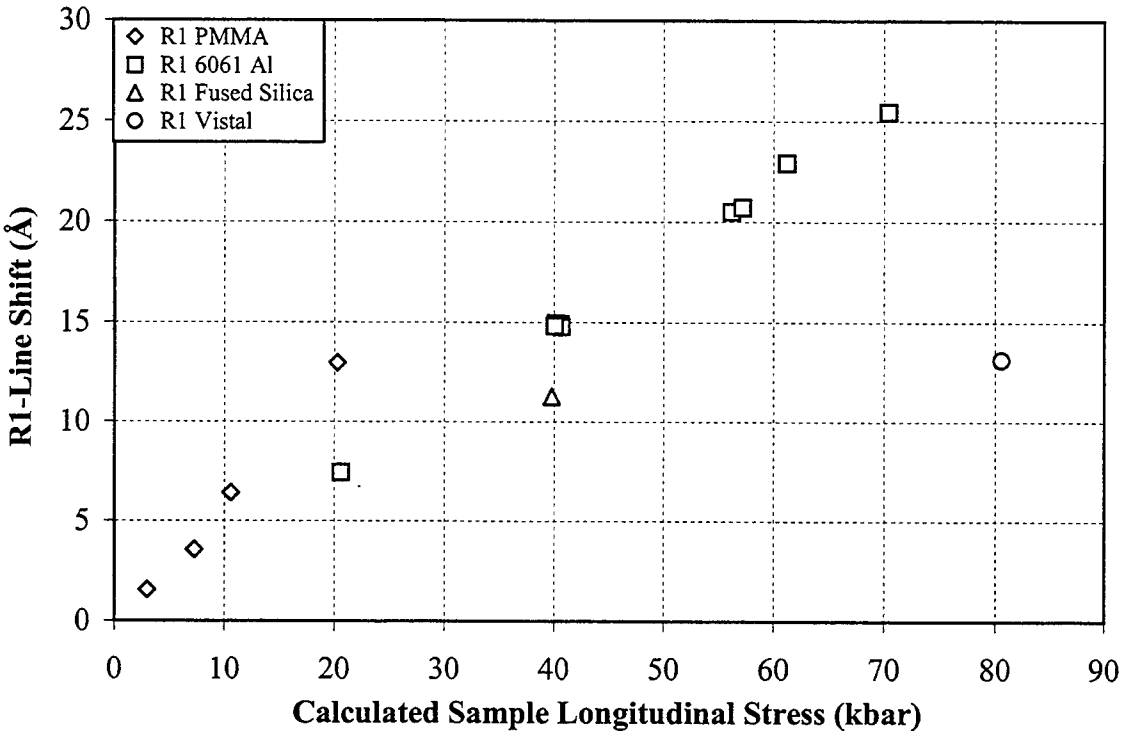

Fig. 6 Summary of R1-line shifts verses sample longitudinal stress.

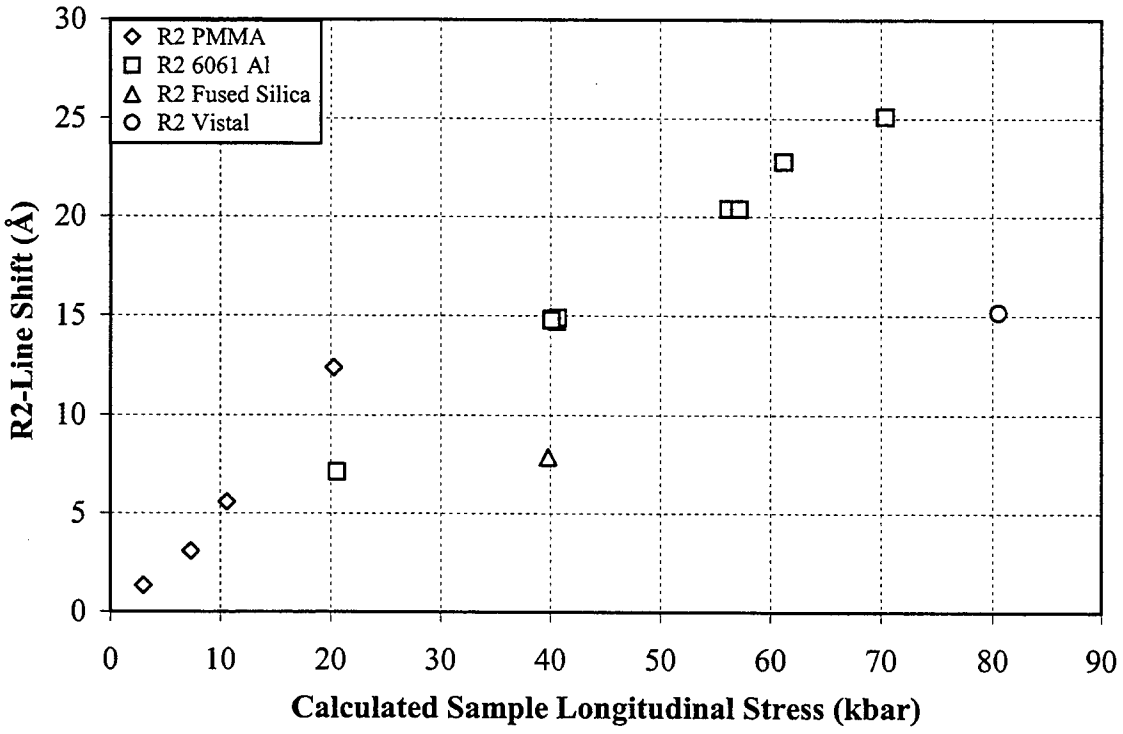

Fig. 7 Summary of R2-line shifts verses sample longitudinal stress.

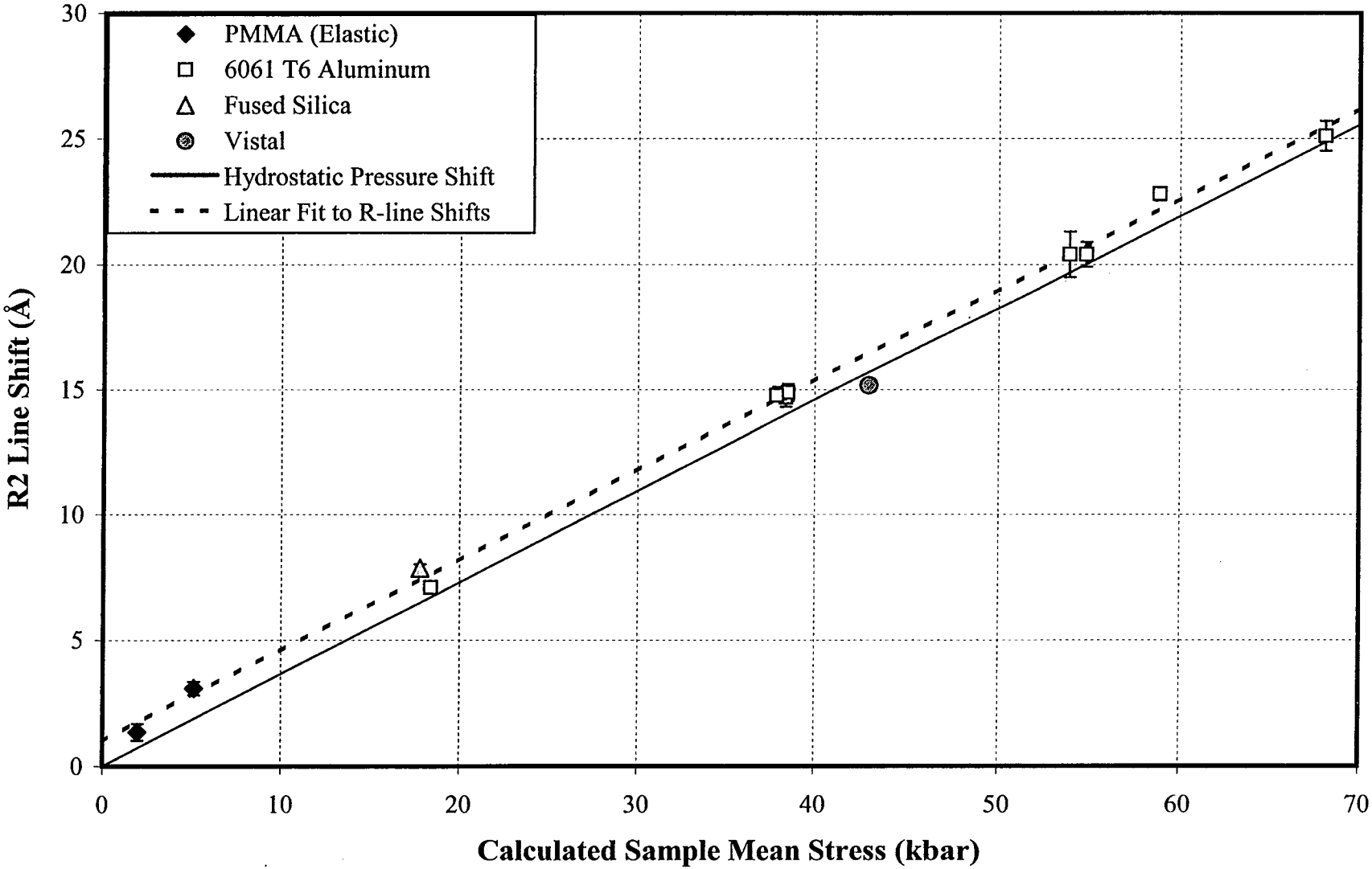

Fig. 8 Summary of R2-line shifts verses sample mean stress corresponding to uniaxial strain loading. The R line shift under hydrostatic compression is also plotted as a reference. The dashed line is a fit to the R2-line shifts.

DISTRIBUTION LIST

DEPARTMENT OF DEFENSE

DEFENSE TECHNICAL INFORMATION CENTER
8725 JOHN J. KINGMAN RD., SUITE 0944
FORT BELVOIR, VA 22060-6218
ATTN: DTIC/OCP

DEFENSE THREAT REDUCTION AGENCY
6801 TELEGRAPH ROAD
ALEXANDRIA, VA 22310-3398
ATTN: CP, DR. D. LINGER
ATTN: CPI, M. FLOHR
ATTN: CPWCT
ATTN: NSSA, W. SUMMA
ATTN: NSSS, C. WELLINGTON
ATTN: NSSS, L. PRESSLEY

DEFENSE THREAT REDUCTION AGENCY
ALBUQUERQUE OPERATIONS
1680 TEXAS STREET, SE
KIRTLAND AFB, NM 87117-5669
ATTN: CPTI, G. LU
ATTN: CPTIE, J. QUINTANA
ATTN: CPTIH, A. VERMA

DEPARTMENT OF DEFENSE CONTRACTORS

APTEK, INC.
1257 LAKE PLAZA DRIVE
COLORADO SPRINGS, CO 80906-3578
ATTN: G. WILLIAMS
ATTN: T. MEAGHER

BOEING DEFENSE AND SPACE GROUP
MISSILES AND SPACE DIVISION
P. O. BOX 240002
HUNTSVILLE, AL 35824-6402
ATTN: DR W. SEIDLER, MS JN-67

HUGHES AIRCRAFT COMPANY
SPACE AND COMMUNICATION GROUP
P. O. BOX 92919
LOS ANGELES, CA 90009
ATTN: L. DARDA, MS-C372 BLDG S25

ITT INDUSTRIES
ITT SYSTEMS CORPORATION
ATTN: AODTRA/DASIAC
1680 TEXAS ST, SE
KIRTLAND AFB, NM 87117-5669
ATTN: DASIAC

KTECH CORPORATION
2201 BUENA VISTA DRIVE, SE, SUITE 400
ALBUQUERQUE, NM 87106-4265
ATTN: D. LEPELL
ATTN: F. DAVIES

LOCKHEED MARTIN CORPORATION
P. O. BOX 3504
SUNNYVALE, CA 94088-3504
ATTN: B. MEENDERING
ATTN: D. E. COX, BUILDING 151, O/V1-40
ATTN: R. SAWYER, BUILDING 158, M1-01

MAXWELL TECHNOLOGIES CO
MAXWELL FEDERAL DIVISION INC.
8888 BALBOA AVENUE
SAN DIEGO, CA 92123
ATTN: DR G. GURTMAN

MAXWELL PHYSICS INT'L CO
2700 MERCED ST
SAN LEANDRO CA 94577-0599
ATTN: R. L. SCHNEIDER
ATTN: S. L. WONG

MAXWELL TECHNOLOGIES
8888 BALBOA AVE., BLDG. 1
SAN DIEGO, CA 92123
ATTN: J. RAUCH

PHYSITRON INC.
3304A WESTMILL DRIVE
HUNTSVILLE, AL 35805-6132
ATTN: R. SKARUPA

SCIENCE APPLICATIONS INTL CORP
2109 AIR PARK ROAD, SE
ALBUQUERQUE, NM 87106
ATTN: R. MILLER

SCIENCE APPLICATIONS INT'L CORPORATION
P. O. BOX 1303
MCLEAN, VA 22102
ATTN: B. L. BEERS

SVERDRUP TECHNOLOGY INC
P. O. BOX 884
TULLAHOMA, TN 37388
ATTN: M. BABINEAU
ATTN: V. KENYON

TEXTRON SYSTEMS CORPORATION
201 LOWELL STREET, ROOM 3289
WILMINGTON MA 01887-2070
ATTN: J. CROWLEY

THE AEROSPACE CORPORATION
P. O. BOX 92957
LOS ANGELES, CA 90009-2957
ATTN: C. CREWS, M5 644
ATTN: L. MENDOZA, M4090

WASHINGTON STATE UNIVERSITY
PHYSICS DEPT
PULLMAN, WA 99164-2814
ATTN: PROF Y. GUPTA

DEPARTMENT OF ENERGY

UNIVERSITY OF CALIFORNIA
LAWRENCE LIVERMORE NATIONAL LAB
P. O. BOX 808
LIVERMORE, CA 94551-9900
ATTN: REPORTS LIBRARY

LOS ALAMOS NATIONAL LABORATORY
P. O. BOX 1663
LOS ALAMOS, NM 87545
ATTN: CIC-14: REPORT LIBRARY
ATTN: S. HAN

SANDIA NATIONAL LABORATORIES
ATTN: MAIL SERVICES
P. O. BOX 5800
ALBUQUERQUE, NM 87185-0459
ATTN: C. COVERDALE, MS 1159
ATTN: C. DEENEY, MS 1194
ATTN: D. BEUTLER/MS 1179
ATTN: J MAENCHEN, MS 1193
ATTN: J. R. LEE, MS 1179
ATTN: M. HEDEMANN, MS 1159
ATTN: R. SPIELMAN, MS 1194
ATTN: W. BALLARD, MS 1179
ATTN: W. H. BARRETT, MS 1159
ATTN: TECH LIB/MS 0899

DEPARTMENT OF THE AIR FORCE

AIR FORCE RESEARCH LABORATORY
3550 ABERDEEN AVENUE, S.E.
KIRTLAND AFB, NM 87117-5776
ATTN: PSO/TL
AIR UNIVERSITY LIBRARY
600 CHENNAULT CIRCLE
BUILDING 1405, ROOM 160
MAXWELL AFB, AL 36112-6424
ATTN: AUL-LSE

OGDEN AIR LOGISTICS CENTER/LMR
BUILDING 1229, 6011 GUM LANE
HILL AFB, UT 84056-5826
ATTN: J. OLDHAM, CHIEF, RS/RV

DEPARTMENT OF THE ARMY

COMMANDER
NUCLEAR EFFECTS DIVISION
DEPARTMENT OF THE ARMY
WHITE SANDS MISSILE RANGE, NM 88002-5176
ATTN: STEWS-NE, J. MEASON

COMMANDER
US ARMY NUCLEAR & CHEMICAL AGENCY
7150 HELLER LOOP, SUITE 101
SPRINGFIELD, VA 22150-3198
ATTN: MONA-AD LIBRARY

US ARMY RESEARCH LAB
AMSRL-SL-CS E3331
5101 HOADLEY ROAD
ABERDEEN PROVING GROUND, MD 21010-5423
ATTN: SLCBR-DD-T, TECHNICAL LIBRARY

US ARMY RESEARCH LABORATORIES
2800 POWDER MILL ROAD
ADELPHI, MD 20783-1197
ATTN: TECHNICAL LIBRARY

DEPARTMENT OF THE NAVY

NAVAL RESEARCH LABORATORY
4555 OVERLOOK AVENUE, SW
WASHINGTON, DC 20375-5000
ATTN: CODE 6615, DR. R. WALTERS

COMMANDER
NAVAL SURFACE WARFARE CENTER
DAHLGREN DIVISION
17320 DAHLGREN ROAD
DAHLGREN, VA 22448-5000
ATTN: TECHNICAL LIBRARY

DIRECTOR
STRATEGIC SYSTEMS PROGRAMS
1931 JEFFERSON DAVIS HIGHWAY
ARLINGTON, VA 22202-3518
ATTN: SP280, CDR D. SCHROEDER